View metadata, citation and similar papers at core.ac.uk
brought to you by CORE
provided by PolyPublie

UNIVERSITÉ DE MONTRÉAL

DESIGN AND IMPLEMENTATION OF A CENTRALIZED DISTURBANCE DETECTION SYSTEM FOR SMART MICROGRIDS

REZA POURRAMEZAN
DÉPARTEMENT DE GÉNIE ÉLECTRIQUE
ÉCOLE POLYTECHNIQUE DE MONTRÉAL

MÉMOIRE PRÉSENTÉ EN VUE DE L'OBTENTION
DU DIPLÔME DE MAÎTRISE ÈS SCIENCES APPLIQUÉES
(GÉNIE ÉLECTRIQUE)
JUIN 2017

© Reza Pourramezan, 2017.

UNIVERSITÉ DE MONTRÉAL

ÉCOLE POLYTECHNIQUE DE MONTRÉAL

Ce mémoire intitulé :

DESIGN AND IMPLEMENTATION OF A CENTRALIZED DISTURBANCE DETECTION SYSTEM FOR SMART MICROGRIDS

présenté par: POURRAMEZAN Reza
en vue de l'obtention du diplôme de: Maîtrise ès sciences appliquées
a été dûment accepté par le jury d'examen constitué de:

M. MAHSEREDJIAN Jean, Ph. D., président
M. KARIMI Houshang, Ph. D., directeur de recherche
M. ZHU Guchuan, Ph. D., membre et codirecteur
M. KOCAR Ilhan, Ph. D., membre

DEDICATION

To my loving parents, Hossein and Parivash
my dear sister Panteha
and my lovely wife Mandana...

ACKNOWLEDGEMENTS

I would like to express my full gratitude to my supervisor Dr. Houshang Karimi and my co-supervisor Dr. Guchuan Zh, who all along this thesis were present to assist me. Providing me with the opportunity to work on this subject and good advice, they guided me towards more challenges in this research field.

I wish to thank Younes Seyedi who helped me developing the core ideas of this thesis and remained available to me throughout all the process.

The support of Vizimax Inc. providing all the equipment and the laboratory to develop this project is greatly acknowledged. I would also like to thank the engineering team I met at Vizimax Inc. for their help and cooperation during the experiments in their facility. Also in Vizimax Inc., all the other employees I have met during this work are acknowledged for the beautiful working environment as well as the welcoming atmosphere, they provided.

Special thanks to Michel Mont-Briant, for his great help in implementing the test setup and analyzing the results. I am also thankful to Jean-Marc Da Pozzo for helping me develop software parts.

Profuse thanks go equally to Dr. Jean Mahseredjian and Dr. Ilhan Kocar for their participation to the jury of this thesis and their review of the text.

RÉSUMÉ

Les micro-réseaux sont soumis à diverses perturbations, telle que l'excursion de fréquence et de tension. La détection des perturbations peut être effectuée par un système de surveillance centralisé de micro-réseaux qui utilise des données de synchrophasor rapportées par différents nœuds. Les réseaux de communication de synchrophasor présentent des retards et des pertes de paquets qui peuvent détériorer l'intégrité des données et, par conséquent, compromettre la fiabilité des systèmes de surveillance et de contrôle des micro-réseaux intelligents.

Ce mémoire présente un nouveau concentrateur des données des vecteurs de phase avancé (APDC) capable de compenser les données perdues et d'améliorer la qualité des ressources de la production décentralisée (DER) dans les micro-réseaux. L'APDC proposé utilise un système de compensation adaptatif pour obtenir une estimation efficace des éléments de données perdus. L'estimateur adaptatif utilise le taux de changement d'éléments de données pour choisir entre l'estimateur linéaire des moindres carrés moyens (LMMSE) et un estimateur basé sur les dérivés pour prédire les valeurs futures des éléments de données. S'il manque , à un instant donné, les éléments de données synchrophasors de certaines unités de mesure de phasor (PMU), les valeurs estimées sont utilisées pour compenser les données perdues. En outre, une unité de surveillance est proposée pour détecter de manière fiable les excursions en fréquence et identifier les DERs affectés par les îlotages. Cette unité de surveillance utilise un algorithme de détection centralisé élaboré qui traite les données de fréquence pour distinguer entre l'îlotage possible des DERs et les perturbations du réseau de distribution.

L'APDC proposé est développé sur la plate-forme OpenPDC en temps réel et sa performance est évaluée à l'aide d'une configuration expérimentale comprenant trois PMUs, un réseau de télécommunications, des interrupteurs, et un concentrateur de données de vecteurs de phase classique (PDC). Les résultats expérimentaux confirment une intégrité des données de haut niveau dans les conditions normales et perturbées des micro- réseaux. Des études sur l'effet du bruit de mesure montrent que l'APDC proposé est même efficace en présence de bruits sévères. De plus, une détection rapide et fiable des événements d'îlotage est obtenue grâce à de l'amélioration considérable du temps de détection même en cas de pertes de données sévères et de bruit de mesure. Enfin, la performance de l'APDC proposé est comparée à une méthode d'estimation existante. Les résultats montrent l'avantage important de l'APDC, en particulier dans des conditions perturbées.

ABSTRACT

Microgrids are subject to various disturbances such as voltage transients and frequency excursions. Disturbance detection can be performed at the level of microgrids by a centralized monitoring system that employs synchrophasor data reported from different nodes within the microgrid. Synchrophasor communication networks exhibit delays and packet dropout, which may undermine the data integrity and hence compromise the reliability of monitoring and control systems.

In this thesis, an advanced phasor data concentrators (APDC) is proposed to mitigate the communication impairments and improve the quality of monitoring of distributed energy resources (DERs). The proposed APDC utilizes an adaptive compensation scheme to achieve an efficient estimation of missing data elements. The adaptive estimator employs the rate of change of data elements to choose between the vector linear minimum mean square error (LMMSE) and the derivative-based estimators to predict the future values of data elements. Whenever the synchrophasor data elements of some phasor measurement units (PMU) are missing, the estimated values are used to compensate for the missing data. Moreover, a monitoring unit is proposed to reliably detect frequency excursions and identify the DERs affected by islanding events. The monitoring unit utilizes an elaborate centralized detection algorithm that processes frequency data to distinguish between possible islanding of DERs and disturbances occurred within the host grid.

The proposed APDC is developed on a real-time OpenPDC platform and its performance is evaluated using an experimental setup including three PMUs, communication links, switches, and a conventional phasor data concentrator (PDC). The experimental results confirm a high-level data integrity under both normal and disturbed conditions. Studies on the effect of measurement noise show that the proposed APDC is even efficient in the presence of noise. Moreover, fast and reliable detection of islanding events is achieved even under severe data losses and measurement noise. Finally, the performance of the proposed APDC is compared with a recently proposed estimation method, which shows a significant advantage of the APDC, especially under disturbed conditions.

TABLE OF CONTENTS

LIST OF TABLES

LIST OF FIGURES

LIST OF SYMBOLS AND ABBREVIATIONS

Symbols

f_n	Nominal Frequency
Δf	Frequency Deviation (Error) From Nominal Value
Δf_T	Defined Frequency Threshold for Islanding Detection
$\gamma(k)$	Phase Angle Estimation Error
$\hat{\text{ROCOF}}(k)$	Estimated ROCOF
$\hat{f}(k)$	Estimated Frequency
$\hat{X}$	Estimated Synchrophasor
$\hat{X}_i$	Imaginary Part of Estimated Synchrophasor
$\hat{X}_r$	Real Part of Estimated Synchrophasor
$\lambda(k)$	Magnitude Estimation Error
$\mathbf{C}_{\hat{\mathbf{x}}\mathbf{X}}$	$P \times PN$ Cross-Covariance Matrix
$\mathbf{C}_{\mathbf{XX}}$	$PN \times PN$ Data-Covariance Matrix
$\mathbf{X}[k\|N]$	Concatenated Data Vector
$\mathbf{x}_i[k\|N]$	Data Vector
ω_n	Nominal Angular Frequency
ϕ	Phase Angle
$\Phi(t)$	Phase Angle of The Synchrophasor
A	magnitude of a sinusoid
$E\left(\hat{\mathbf{x}}\right)$	Expected Value of Predicted Data Vector
$E\left(\mathbf{X}\right)$	Expected Value of Actual Data Vector
f	Frequency
F_s	PMU Reporting Rate
k	An Instant in Time
N	Defined Number of Data Samples in The Estimation Window
T_n	Nominal Period of The Power System
x	sinusoidal signal
$X(t)$	synchrophasor representation of a sinusoid
$X_i(t)$	Imaginary Part of The Synchrophasor
$X_r(t)$	Real Part of The Synchrophasor
x'_T	Defined Threshold for Rate of Change of Parameter

Abbreviations

APDC	Advanced Phasor Data Concentrator
DER	Distributed Energy Resources
CRC	Cyclic Redundancy Check
CS	Compressive Sampling
CSC	Current Symmetrical Components
CSD	Critical Slowing Down
DG	Distributed Generation
DS	Distributed Storage
EMS	Energy Management System
ESP	Event Stream Processor
FE	Frequency Measurement Error
fps	Frame Per Second
FRACSEC	Fraction of a Second
GOOSE	Generic Object Oriented Substation Events
GPA	Grid Protection Alliance
IDE	Integrated Development Environment
IRIG-B	Inter-Range Instrumentation Group Time Code
I/O	Input/Output
LC	Local Controller
LIFO	Last In First Out
LMMSE	Linear Minimum Mean Square Error
LOF	Local Outlier Factor
LPF	Low Pass Filter
MCC	Microgrid Central Controller
MSE	Mean Square Error
NaN	Not a Number
NCD	Number of Consecutive Detections
NERC	North American Electric Reliability Corporation
NTP	Network Time Protocol
PC	Point of Connection
PCC	Point of Common Coupling
PDC	Phasor Data Concentrator
PDF	Probability Density Function
PLC	Power Line Carrier

PMU	Phasor Measurement Unit
PPS	Pulse Per Second
PTP	Precision Time Protocol
PV	Photovoltaic
RFE	ROCOF Measurement Error
ROCOF	Rate Of Change Of Frequency
SCADA	Supervisory Control And Data Acquisition
SOC	Second Of Century
TVA	Tennessee Valley Authority
TVE	Total Vector Error
UTC	Coordinated Universal Time (French: Temps Universel Coordonné)
WAMS	Wide Area Monitoring System

CHAPTER 1 INTRODUCTION

1.1 Microgrids and wide area monitoring systems

The modern power system is moving towards increasing use of microgrids for a more economical operation. The reliability and security of smart microgrids and the host electrical power system are the new challenges for power system designers [1, 2]. Implementation and development of smart microgrids require various improvements in the operation and control systems of existing microgrids. One essential improvement is the integration of synchrophasor data, energy management systems, and protection/control systems to the microgrid. The accuracy of the data provided to these systems plays a major role in their efficiency.

Distributed energy resources (DERs) consisting of both distributed generation (DG) and distributed storage (DS) units with different capacities and properties, are increasingly deployed in electric power utility grids. The integration of DER units into the electric power grid has brought about the concept of smart microgrids [3]. However, DER units based on renewable energy sources, e.g., wind and solar, give rise to new challenges regarding power system management, protection, and control [4]. Figure 1.1 shows the schematic diagram of a typical microgrid. A microgrid is a local electric power system consisting of DER units, loads, and energy storage systems. Microgrids supply the power demanded by a variety of clients, e.g., residential buildings, commercial centers, and industrial parks. The microgrid is usually located at the downstream of a distribution substation and is a part of the electric power distribution system [3].

The microgrid and the utility grid are normally connected electrically together at the low-voltage side of the substation transformer which is called the point of common coupling (PCC). The mode of operation with which the microgrid is connected to the utility grid through the substation transformer is called grid-connected mode [4]. A microgrid subjected to different types of faults or utility outage may partially or completely be disconnected from the host grid. When a microgrid is disconnected partially or completely from the host grid, a power island is created [5]. In the islanded mode, the microgrid should remain operational as an autonomous entity, maintain some level of service, and provide sufficient generation capacity and controls to supply a portion of its local load. Traditionally, some power utilities consider accidental islanding events and automatic resynchronization of the microgrid as undesirable conditions due to safety, equipment protection, and system stability concerns. Attempts were made to address these issues through anti-islanding features provided in DER units and other practices recommended by standards such as the IEEE 1547

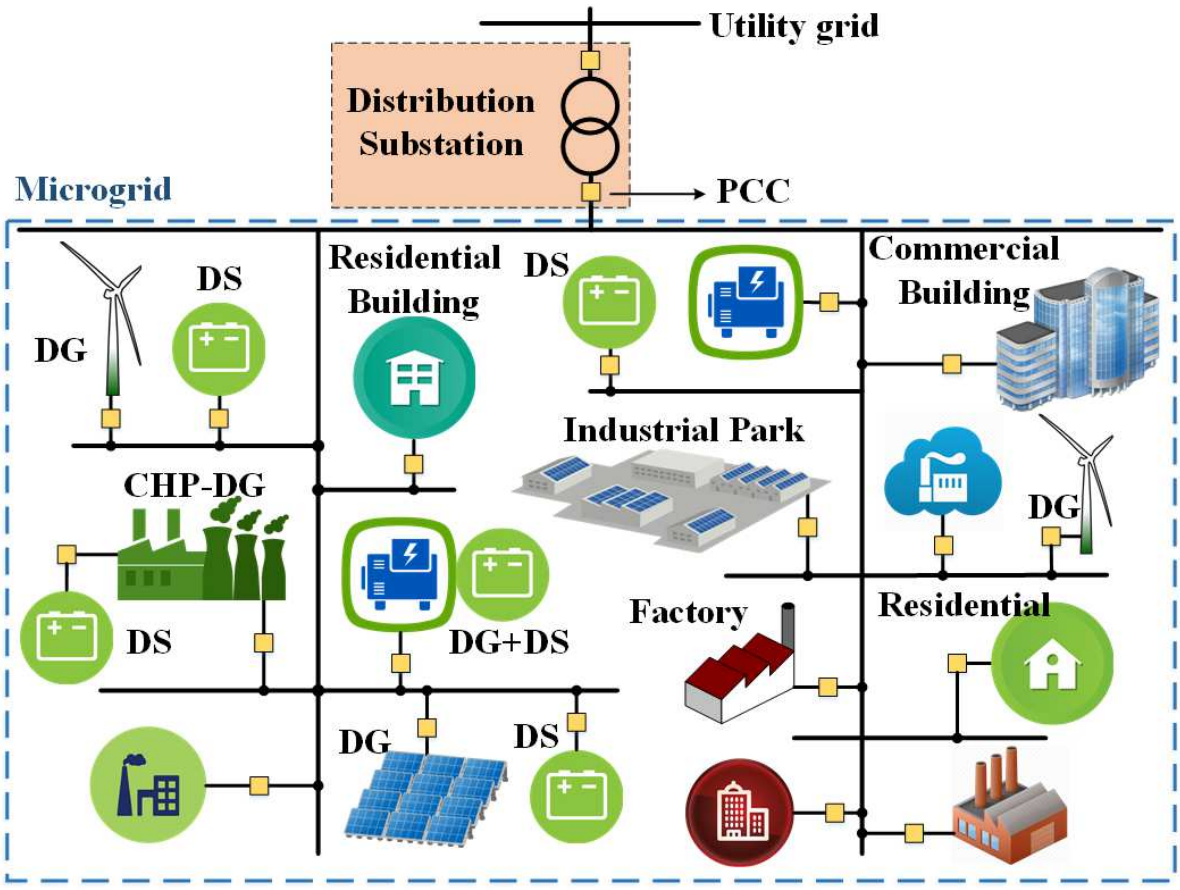

Figure 1.1 The structure of a typical microgrid including DER units and loads.

standard [6]. However, large number of DERs installed in the power system together with the recent advancements of electronically-coupled DER units require arrangements for both grid-connected and islanded modes of operations to be effective.

Moreover, the transition between the two modes of operations should be carried out smoothly and efficiently to facilitate the optimal utilization of the microgrid. An effective approach is to switch to autonomous operation mode when the microgrid is disconnected from the main grid, [7]. In the autonomous mode, the loads can be supplied using the available DERs within the islanded zone. However, it may require load shedding to balance the power between generations and consumptions. To provide smooth transition from grid-connected mode to islanded mode and to guarantee continuous supply for the critical loads, fast, accurate and reliable detection of the islanding event using a centralized monitoring mechanism is required [8].

Several islanding detection schemes have been proposed in the literature [9]–[13]. However,

the proposed islanding detection methods do not possess all the key features such as effectiveness, reliability, minimality of infrastructure requirements, and applicability to any DER technology. The islanding detection methods can be categorized into passive, active and communication-based methods. Passive islanding detection methods rely on the local measurements of DER units, have low-cost and are applicable to all DER technologies. However, these methods suffer from non-detection zone (NDZ) and false tripping [14]. Active islanding detection schemes inject a small disturbance signal to the grid through the DG control system and detect the abnormalities at the PCC subsequent to the grid disconnection. Active methods are more reliable and their NDZs are smaller as compared to those of the passive methods [13]. However, these methods are more expensive and in many cases are not applicable to all DER technologies. The communication-based methods monitor the state of circuit breakers between the DERs and the grid, and identify the islanding event. Although these methods are expensive, they offer an excellent performance in terms of detection time and NDZ. Any passive or active anti-islanding scheme is based on some threshold that crossing which will indicate an islanding event. Due to the existence of these threshold values, any passive or active method may introduce an NDZ in which it fails to detect the islanding event. For example, in passive methods that use under/over frequency and/or under/over voltage, the NDZ is defined as the small power mismatch space of the connected mode and islanded mode where the frequency and voltage deviation is not large enough to trigger the detection algorithm [15].

DER units can be classified into two groups in terms of their interface to the microgrid [3]. The first group consists of conventional rotating electrical machines that have similar dynamic behaviors as the conventional utility grid. The second group includes electronically coupled DER units that use converters to provide an interface to the utility grid. The dynamic behavior and control concept of these two groups are fundamentally different. Therefore, the control strategies and techniques employed for an autonomous mode microgrid (islanded mode of operation) are considerably different from those of the conventional utility grid. Furthermore, contrary to the traditional controls and energy management systems of interconnected power systems, control and management systems for microgrids are mostly the types of control and power/energy management strategies for a microgrid are mainly designed based on the conditions of the microgrid, the adopted DER technologies, and load specifications. Therefore, adequate robust controllers should be designed and utilized to guarantee voltage and frequency stability of the islanded zone despite loads uncertainties and source variations [16, 17].

Figure 1.2 shows a DER unit including a distributed energy source, an interface device that enables the connection between the source of energy and the microgrid, and a connection

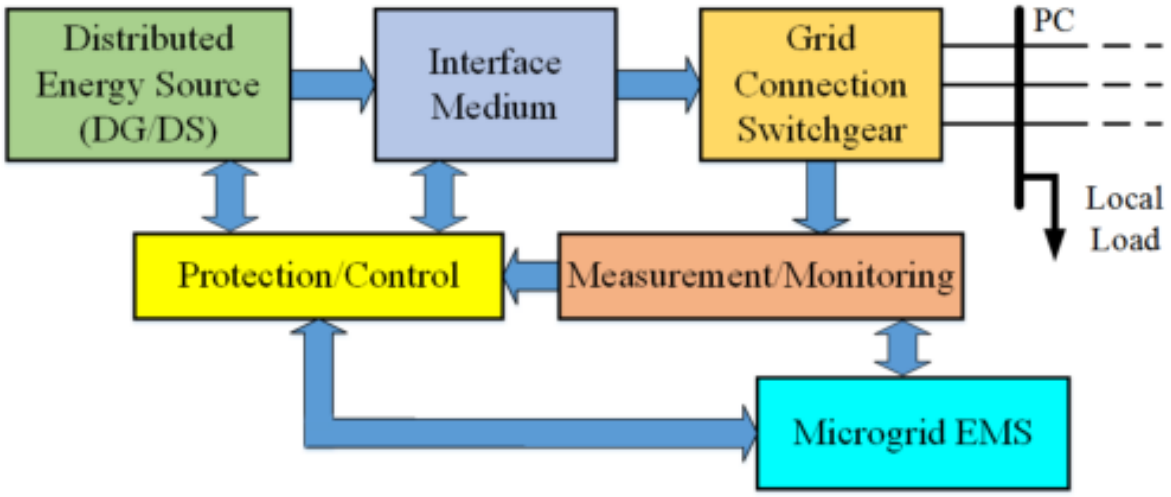

Figure 1.2 General block diagram of a DER unit connected to the rest of the microgrid.

switch at the point of connection (PC) where the DER unit connects to the rest of the microgrid [3]. The distributed source of energy can be either a DG or a DS. The DG unit itself can be a conventional rotary machine (e.g., a synchronous generator or an induction generator) or an electronically coupled DG (e.g., converter-based renewable energy resources). Rotary machines provide the electrical power and also act as the interface medium between the source of energy and the microgrid. If an electronically coupled DG unit or a DS unit is adopted, a converter should be employed as the interface device, which adds an extra layer of energy conversion, monitoring, and control to the DER unit. In addition to the above mentioned DER units, hybrid DER units that include both DG and DS as the primary energy source and the storage device, respectively, are also available. The interface layer for hybrid DER units is usually a bidirectional AC/DC converter. The switchgear in Figure 1.2 can include transformers and low-pass filters (LPF) and facilitates the connection of the DER unit to the rest of the microgrid at the PC [16]. Measurement devices and monitoring units are installed at the PC. The measured data are sent to protection/control units that control the energy source and the interface devices for electronically coupled DG/DS units.

The energy management system (EMS) of a microgrid is responsible for assigning real and reactive power references to the DER units [18]. The EMS receives real-time actual and estimated measurements of DER units and loads along with the market information to determine and control the desired power references to DER units, power flows, the controllable loads, and the consumption level of the utility grid. Due to the presence of multiple DER units that often have fast transient responses, the EMS must have a quick response comparing to conventional power system management systems.

The EMS collects the data of both measurement/monitoring and protection/control units and can send commands to them. The loads supplied by a microgrid can be both electrical or thermal loads. In grid-connected mode, the utility grid acts as an infinite bus and compensates for any power discrepancy in the microgrid by either supplying the missing electrical power or absorbing the surplus power produced by the microgrid. Therefore, the load/generation balance of the microgrid is maintained in grid-connected mode. However, in islanded mode of operation, load/generation shedding is usually needed to achieve the load-generation balance and to maintain frequency, voltage, and angle stability. The operating strategies of the microgrid should guarantee that the sensitive loads are supplied. Moreover, power quality and reliability of the microgrid are considered as important issues.

The EMS should support both short-term and long-term energy management requirements [18]. The responsibilities of short-term energy management include voltage regulation, frequency control, supplying the demands of variable loads, providing desired power quality for sensitive loads, stabilizing the frequency/voltage of the microgrid during and following to events that create transients, and facilitating synchronized reconnection to the main grid following an islanding. The long-term energy management requirements include controlling the net power import/export from/to the utility grid, minimizing the cost of power generation, optimizing the power output of renewable energy resources, and determining the conditions and limitations of individual DER units (e.g., maintenance intervals and operational costs). Determining and maintaining an appropriate reserve capacity for the microgrid and restoring the loads that are disconnected intentionally or followed by an event are also considered as long-term responsibilities of the EMS.

The long-term and short-term objectives of microgrids are obtained through microgrid supervisory control that usually has three layers of hierarchy and can have either a centralized or a decentralized structure [4]. Figure 1.3 shows the typical structure of the microgrid supervisory control system intended for a distribution network with several microgrids. The lower layer of control consists of the local controllers (LC) of individual DERs or loads. The middle layer includes microgrid central controllers (MCC) that are responsible for individual microgrids. Finally, the higher level of the hierarchy includes the distribution network operator (DNO) and the market operator (MO) that supervise several microgrids serving the distribution power system [7]. The DNO manages a distribution network with several microgrids, and the MO is responsible for the marketing management of a particular area in the distribution network.

In a microgrid with a decentralized MCC structure, each LC acts individually based on the local measurements [19]. The decentralized control strategy aims at providing the maximum

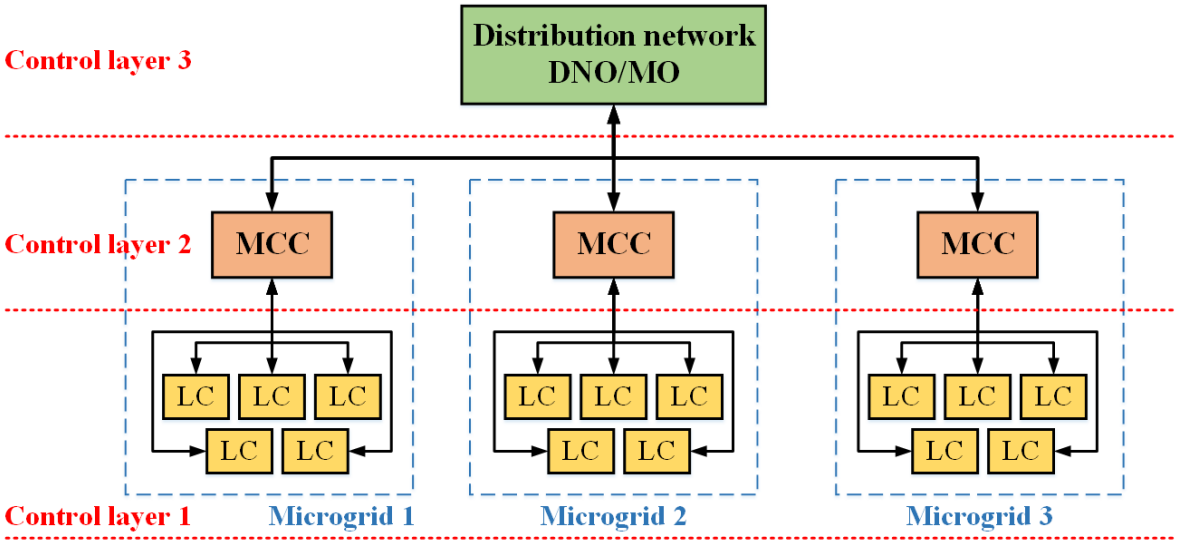

Figure 1.3 Hierarchy structure of the microgrid supervisory control

independence for the intelligent LCs that can communicate with each other within a microgrid. In a microgrid with a decentralized control system, the primary objective of individual controllers is to enhance the overall performance of the microgrid without considering the economic efficiency of individual DER units. However, in a microgrid with the centralized structure, the MCC can impose new set points to each LC that can override the decision made by LCs. In a centralized control system, the MCC optimizes the level of the power imported/exported from/to the main grid and improves the revenue of the individual DER units [3].

Different smart grid technologies can be used to establish the communication between LCs, MCC and DNO/MO units [20]. Early communication technologies, e.g. telephone lines and power line carriers (PLC), have many limitations. While wireless communication is considered for future distribution automation applications, fiber optic communication networks are considered as the most reliable technology. It should be noted that even in the decentralized control structure, the reliability and the performance of the communication system between LCs is an essential issue. Centralized control and protection of DER units require a reliable monitoring mechanism to detect potential islanding events in a timely manner.

Phasor measurement units (PMUs) are devices capable of measuring the voltage and current phasors, frequency and the rate of change of frequency (ROCOF) of a three-phase system with a reporting rate of typically 10, 30 and 60 samples per seconds [21]. The dynamic events of the measured system can be studied up to a frequency of half of the reporting rate. The reference for measuring the phase angle of the phasors is received from a source of time such

as a GPS clock and therefore all the measurements are indicated by a timestamp that allows the synchronization of the data of several PMUs. The synchronized phasors measured by PMU are called *synchrophasor* and have an accuracy in range of one microsecond.

PMU generates synchrophasor data and report them to a phasor data concentrator (PDC) via communication links [22, 23]. PDCs are used to collect and synchronize the data of several PMUs, and to produce synchrophasor data sets which are then transmitted to centralized monitoring and control systems at different levels. Since all the measurements have a timestamp acquired from reliable time reference, the PDC can align the measurements chronologically. Additionally to a data concentrating device, PDCs can be configured for various applications, e.g., storage and archiving PMU data, and performing power system calculations and analyses.

Wide area monitoring systems (WAMS) are primarily based on the synchrophasor measurements and enable monitoring of the power system across wide areas for the purpose of analysis, event detecting and preventing possible grid instabilities [18], [21]. The synchrophasors with the same timestamps provide snapshots of the condition of the power system monitored nodes. Both steady-state and dynamic behavior of various nodes in different voltage levels of the power system can be monitored by comparing the snapshots with each other. With the increasing deployment of PMUs in power systems, the utilization of WAMS to collect data from multiple PDCs and to facilitate the supervisory control of microgrids, is growing. One of the objectives is the fast detection of disturbances occurring in remote areas and possible instabilities. A WAMS can also gather the geographical information of different parts of a power system and provide a geographic visualization that is a significant improvement comparing to the conventional EMS displays. Nowadays, with the penetration of DER units, new dynamics and complications are introduced to the distribution networks. Therefore, the utilization of synchrophasor measurements in WAMS applications is growing more compelling.

One of the concerns in designing WAMS is site selection to install PMUs [24]. The intended application determines the minimum number of PMUs, and the total cost and available communication facilities restrict the number of PMUs to be installed. Therefore, an optimal PMU placement is essential to meet the requirements of both intended applications and cost criteria [25, 26]. Recently, micro-phasor measurement units (μPMU) are developed for measurements at consumer voltage level. μPMUs are less costly than conventional PMUs and can improve the penetration and the effectiveness of WAMSs in modern power systems [27]–[29]. Using μPMUs and increasing the points of measurements of the WAMS can significantly improve the monitoring resolution of distribution networks and microgrids. On the other

hand, the conventional management, control, and protection of distribution networks utilize mainly voltage/current magnitude measurements.

Synchrophasor-based applications need reliable, secure and fast communication networks [30]. Power systems often use dedicated networks for synchrophasor measurement communications. PMUs are usually installed in remote substations far from super-PDCs. On the other hand, communication network infrastructures and bandwidth requirements increase by growing the number of installed PMUs in WAMS. Therefore, the required dedicated communication networks are expensive to construct, expand, and maintain. PMU reporting rate is mainly restricted by the bandwidth capacity of the WAMS [21]. Hence, synchrophasor communication links with high reporting rates are not economically feasible for many power systems and especially for distribution networks. However, many protection and control applications in WAMS require high-rate synchrophasor data. Moreover, in a WAMS, the synchrophasor communication system can experience impairments such as excessive delays, and single or a series of consecutive data packet dropouts. These communication impairments can falsify the results of critical applications such as event detection. The same problem can occur when the PMUs produce bad synchrophasors data in some circumstances.

1.2 Related work to synchrophasors applications in smart grids

Many applications of synchrophasor data in WAMSs and microgrid monitoring have been discussed in the literature [18], [21]–[23], [31]. However, the effects of communication impairment and bad synchrophasor data have not been fully addressed by the literature and no comprehensive method is proposed to solve these issues.

In [18], several proactive synchrophasor solutions for smart grids are discussed. It has been shown that the synchrophasor data can be effectively used in archived grid data for post-event analyses, fast and improved monitoring of grid disturbances, detecting disturbances external to one's region, islanding detection, and substation state estimation. Moreover, symbiotic integration of synchrophasor data into fast action controls in smart grids is introduced. It is shown that the synchrophasor data can be efficiently integrated into existing systems local substation controls, renewable energy system controls, predictable net energy systems in microgrids, and future EMSs.

In [21], several applications of synchrophasor data in power system monitoring, protection, and control are introduced. Power system monitoring includes post-event monitoring, WAMS, state estimation, and frequency monitoring network (FNET). Three applications of PMU data in protection functions with relatively slow response times are represented. These

applications are control of backup protection of distance relays, protection functions related to angular voltage stability, and detection systems where dependability and security could be reevaluated based on the stress of the system. Finally, the application of synchrophasor data and WAMS in centralized control schemes is discussed. In [31], several applications such as data acquisition and monitoring, fault detection, state estimation, and dynamic monitoring are reviewed.

A synchrophasor-based approach is proposed to resynchronize microgrid with the utility grid with a smooth transition from islanded mode to grid connected mode [32]. In the proposed method, the voltage phase angle mismatch of the circuit breaker/recloser at PCC and the utility grid is eliminated using a digital PI controller to avoid out-of-phase reclosing. Several islanding detection methods have been proposed in the literature [9]–[13], [33]–[37]. All of the proposed methods are based on the observation of power system measurements (i.e. frequency, voltage, and/or current). It should be noted that the imperfect data transmission may result in higher detection times that can lead to instability of the islanded microgrid.

In [35], the most widely used passive islanding detection methods (i.e. under/over frequency detection, under/over voltage detection, and phase jump detection) are studied and compared using the power mismatch NDZ as the performance index for evaluation. The methods are tested on a simple test system including a single inverter-based DG connected to the grid and an RLC load. The results show that both under/over frequency detection and under/over voltage detection methods have large NDZs. For inverter-based DGs, the NDZ of under/over frequency method is dominated by reactive power mismatch while active power mismatch dominates the NDZ of under/over voltage method. The NDZ of the phase jump method is very sensitive to the increase of its threshold. However, unlike the under/over frequency method, the NDZ of the phase jump method is independent of the load's quality factor. The NDZ of the phase jump method is insensitive to active power mismatch (similar to that of the under/over frequency method). Moreover, using the phase jump method and a small phase threshold of the order of few degrees, some power system protection actions (e.g. switchings that do not result in islanding) can lead to false islanding detections. It should be noted that the NDZs were evaluated using steady-state results. If the DG response to islanding takes a long time (more than 2 seconds) to settle, then the NDZ will be even larger than normal.

Authors in [36] evaluated the performance of active frequency drifting islanding detection methods and compared them with the passive frequency drifting islanding detection approach. It has been concluded that the slip mode frequency shift and the and Sandia frequency shift islanding detection methods can be designed to guarantee the islanding detection for an RLC load with a low quality factor. However, for loads with higher quality factors,

the effectiveness of the under/over frequency passive method is comparable with those of active methods. Moreover, the active frequency drift islanding detection method has always an NDZ for all values of the load's quality factor.

In [37], PMUs installed in WAMS are used to detect islanding events using frequency drift and phase jump methods. The frequency drift method locates the nodes where the frequency deviation from a reference frequency has exceeded a threshold for a specific amount of time. The method is tested on the FNET that is a WAMS with several PMUs available. The reference frequency is calculated as the median frequency measured by all the PMUs. The threshold values for frequency and time were set, based on experience, to 20 mHz and 3 s. The results show that the proposed method can accurately detect power system islanding events and will not falsely alarm frequency excursions caused by other events (e.g. generation trips, load shedding, etc.). The frequency threshold and subsequently the NDZ are reduced due to the long time threshold. However, the proposed islanding detection system is not fast enough for quick action applications (e.g. some control and protection actions) [38]. Another drawback of the proposed method is the use of median for determining the reference frequency. Although it can be effective for the detection of islanding events in power system where three are many PMUs installed, it may fail in microgrids where most of the measured nodes are within the microgrid and are subjected to islanding. Even in power systems, if a great number of measurement nodes are within the islanded region, the proposed reference frequency is not an adequate reference.

It has been shown in the literature that the synchrophasor data can be effectively used in centralized monitoring and detection applications. In [39], an interpolative algorithm for data concentration to enhance disturbance detection in smart microgrids is proposed. Although the proposed algorithm can significantly diminish data noise, it may lead to slow response during the microgrid transients. In particular, if all communication links incur packet dropout, then the method replaces missing data with the most recent samples. Under such circumstances, the data concentration becomes recursive which impedes fast detection of time-critical disturbances. Moreover, the proposed method is not applicable to scenarios where only a portion of the microgrid is subject to severe disturbances. Finally, it should be noted that the existing data concentration and detection methods are not validated based on realistic and real-time synchrophasor data.

In [40], real-time synchrophasor data are employed to update a criterion for microgrid event detection dynamically. An autoregressive model-based method for secondary monitoring of DG units is proposed to overcome the lack or failure of communication between some DG units and the MCC. The autoregressive model of the synchrophasors of current symmetrical

components (CSC) at the PCC is extracted using a parameter estimator. An adaptive algorithm uses the autoregressive model to identify the sudden changes in DGs' parameters by evaluating the norm of forwarding prediction error. The proposed method estimates the number of operational DGs in specified time intervals. The MCC uses this data to determine the total generation capacity of the microgrid. The proposed method is evaluated using MATLAB/Simulink simulations of a benchmark with four photovoltaic (PV) units and only provides an estimation of total generation changes in the microgrid. However, the proposed approach strongly requires high-quality PMU data. If the PMU data is lost or corrupted at certain time instants, the algorithm will fail for the those specified instants. Therefore, a compensation method is required to ensure the PMU measurement integrity.

It is shown in [41] that critical transients and possible instabilities (e.g. voltage collapse) in power systems can be detected using time series synchrophasor data. The dynamics of complex stochastic systems before any transition show a statistical pattern of increased recovery times from disturbances, increased signal variance from the mean trajectory, and increased flicker in the signal. These patterns are referred to as critical slowing down (CSD). The CSD properties of data from stochastic dynamical systems are useful to indicate situations when a system is close to a critical transition, collapse, or tipping point. The proposed method in [41] detects critical slowing down (CSD) in the stream of synchrophasor measurements. In this algorithm, a window size is chosen for the calculation of variance and autocorrelation of power system signals (i.e. voltage magnitude, phase angle, or frequency). The data are filtered in each window to exclude slow trends that are not a result of CSD. Both the variance and the autocorrelation of power system signals that are used as metrics of this approach are then calculated. The autocorrelation of the detrended signal is measured using an auto-regressive model. Using Kendall's coefficient, the metrics are verified at one-minute intervals to detect any statistically significant increases. The detection system predicts the time to critical transition with high accuracy, particularly when the critical transition is approaching. It is shown that the predictive ability of the proposed method is more efficient for larger power systems. The proposed method does not require power system models and only relies on the synchrophasor data.

The main drawback of the proposed method in [41] is that the authors assumed that excessive delays and packet dropouts in PMU data can be detected and filtered out of the data streams. Therefore, no method is proposed to compensate for communication losses. This method requires the use of multiple synchrophasor data streams (measurement redundancy) to avoid the effect of communication impairments (if there is no compensating method). In this method, sudden jumps in synchrophasor data (e.g. jumps resulted from islanding events or line tripping) are filtered out using the detrending procedure. Although the detrended signal

could be verified for CSD, the islanding events and line outages cannot be detected using the same data streams.

In [42], the compressive sampling (CS) theory is used to reduces the communication network bandwidth requirements of WAMS. In this method, the synchrophasor data is compressed to a low reporting rate at the sending end of the communication link and is reconstructed at the receiving end to a higher reporting rate. It is shown that the CS algorithm is not severely affected by a limited synchrophasor missing data and bad PMU data. However, no dedicated algorithm for synchrophasor data compensation is presented and the reconstructed data duplicates the same missing data and bad PMU data at the receiving end. The maximum number of the missing data tolerated by the CS algorithm is limited and the effect of consecutive missing data frames is not studied.

In [43], an online data-driven method to detect low-quality PMU measurements is presented. This method depends on the availability of synchrophasor measurements of a region of the power system. Therefore, several PMUs must be installed in a region to provide the method with synchrophasor data of the same type (i.e. voltage, current, and power). It has been shown that the low-quality synchrophasor measurements of particular nodes show weak spatial similarities with the synchrophasor data obtained from PMUs at nearby nodes at the same period. Moreover, the low-quality synchrophasor data of a particular time period presents inadequate temporal similarities with the data of adjacent time periods. The spatial and temporal similarities between synchrophasor measurements of different nodes and time periods are combined and employed to develop an algorithm to detect the low-quality PMU data. Two similarity metrics are defined to detect low-quality synchrophasor data that have higher or lower variance comparing to the spatiotemporal neighborhood. The normalized standard deviation of the synchrophasor data of a particular PMU at a particular time period is used to determine these two metrics. Based on the defined similarity metrics, the proposed algorithm utilizes the local outlier factor (LOF) analysis that is a density-based outlier detection method to verify the reliability of the synchrophasor data of a certain PMUs at each time period.

The proposed method in [43] can satisfactorily detect the bad low-quality synchrophasor data in normal conditions. The authors claim that the algorithm has also a reliable performance under fault-on conditions. However, the simulation results under fault-on conditions are not clear. The main drawback of this method is the effect of the chosen time period on the reliability of the detection algorithm. A longer time window enables more reliable detections whereas a short time window enables faster analysis and exhibits shorter detection delays. Moreover, the method requires high synchrophasor measurement redundancy to achieve bet-

ter accuracy in low-quality data detection. Therefore, the lack of measurement redundancy (i.e. fewer installed PMUs) and/or strong electrical connections among neighboring nodes may lead to false or missed detections. Moreover, the method did not take into account the possible communication packet dropouts and excessive delays. Another drawback of the proposed method is that no attempt has been made to compensate for bad/low-quality PMU data. Therefore, the operators will only have the information on the quality of the synchrophasor data at specified time intervals and cannot rely on a consistent high-quality data for fast applications such as protection and control.

1.3 Thesis objectives and methodologies

The main problems addressed by this research are:

- The effects of communication impairments on the performance of the microgrid monitoring and management system.
- The possibility of proposing a method to compensate the lost and bad synchrophasor data transmitted via communication links.
- The abilities of the proposed communication impairment compensation method in improving the performance of microgrid controllers.

In this thesis, an advanced PDC (APDC) is designed and implemented on a real-time software platform, which improves data integrity and facilitates monitoring of DERs in microgrids. The proposed APDC consists of three fundamental units: a conventional PDC, an estimation/compensation unit, and a monitoring/detection unit. The conventional PDC subsystem collects and aligns the received synchrophasor data streams. The estimation/compensation unit includes an adaptive estimator in order to compensate for data losses, PMU failures, and excessive communication delays. The monitoring/detection unit employs PMU data of the entire microgrid along with the host grid and can be configured in different ways to perform several applications (e.g. monitoring and data visualization, data analysis and energy management, event detection and alarming, control, and protection).

Fast and accurate detection of islanding events is one of the most challenging applications in microgrids, particularly, if communication impairments compromise the data integrity. Therefore, in this thesis, the performance of the proposed APDC is evaluated for islanding detection. Moreover, to verify the performance of the APDC, the frequency and ROCOF data measured by PMU, that are vulnerable to noise and transients, are used as data inputs to the monitoring/detection unit.

The specified objectives of this thesis are as follows:

- Propose an APDC that includes three fundamental units: a conventional PDC, a compensation unit, and a monitoring unit.
- Design an adaptive parameter estimator algorithm that compensates for missing data frames in case of communication impairments. The adaptive estimator applies either a Linear Minimum Mean Square Error (LMMSE) estimator or an estimator based on the rate of the change of the parameters.
- Design an islanding detection algorithm based on frequency excursion detection. The islanding detection unit is designed as a part of the monitoring-detection unit.
- Implement a test setup consisting of three commercial PMUs installed at distribution network voltage level, communication links, and hardware/software PDC.
- Implement the proposed APDC on the *OpenPDC* platform and employ it to collect and process the real-time PMU data of the test system.
- Employ the APDC to validate the proposed method using real-time PMU data. Perform both dynamic parameter estimation and islanding detection in presence of communication impairments to verify the effectiveness of proposed algorithms.

The main contributions of this thesis have been reported in a journal paper published in the IEEE Transactions on Industrial Informatics [44]. More specifically, the contributions and achievements are as follows:

- Proposing a linear/derivative-based adaptive estimator that is used to predict the missing or bad PMU data elements. Using the proposed adaptive estimator, the integrity of output synchrophasor data sets is maintained under both normal and disturbed conditions of the microgrid.
- Proposing a monitoring/detection unit for the APDC that distinguishes disturbances in the voltage magnitude/frequency of the microgrid from those of the main grid. Moreover, using the proposed monitoring/detection unit, the APDC can identify the islanded region and its operating DER units. Such real-time information can significantly improve the performance of centralized protection and control applications in smart microgrids.

1.4 Thesis outlines

The thesis is organized as follows:

In Chapter 2, synchrophasor definition and standards, PMU structure and performance criteria, and PDC structure, configurations, and applications are presented. Moreover, the OpenPDC manager that is used as the test bed of the thesis is introduced.

In Chapter 3, the proposed APDC along with its two sub-units, i.e. estimation/compensation and monitoring/detection units, are presented. The theories, methodologies, and algorithms are discussed in details.

In Chapter 4, the test setup is described and the experimental results of parameter estimation and islanding detection are presented. The experimental results based on the measured PMU data confirm that the proposed APDC enables fast and reliable event detections in the presence of severe communication impairments and noise.

Finally, Chapter 5 summarizes the work reported in this Thesis.

CHAPTER 2 PHASOR MEASUREMENT UNIT AND PHASOR DATA CONCENTRATOR

Wide area measurement system (WAMS) is a technology that allows various applications of the power system to obtain the data of different parts of a large power system and to extract the value of the data. If the wide area real-time synchronized data are available, a continuous monitoring of the power system allows taking immediate action as soon as an event occurs. In such a system, data acquisition is accomplished by digital data recorders capable of producing high-volume, high-quality data streams. The data acquisition system extracts and processes power system data using different algorithms and signal analysis tools. There are several differences between WAMS and supervisory control and data acquisition (SCADA). The SCADA can only provide steady-state, low rate and non-synchronized data of the network [18]. Therefore, management and control centers do not have access to the dynamic states of the power system and cannot take immediate actions in case of events such as faults and failures. However, WAMS provides the management and control centers with synchronized, high-resolution data corresponding to the dynamic states of the power system.

Phasor measurement units (PMU), phasor data concentrators (PDC) and communication links are the fundamental components of a WAMS. PMU is a measurement device that uses synchronizing signals to provide the voltage and current phasor measurements along with the frequency and the ROCOF of a node in the power system. PMUs are the first layer of the WAMS, while PDC can be found at higher levels as a node where the data of several PMUs or other PDCs are correlated and streamed out as a single data stream useful for power system applications.

In this chapter, the concepts of synchrophasor measurement, frequency and ROCOF are introduced. The synchronization and time tagging processes that are required for synchrophasor measurements are described. Moreover, the phasor measurement unit (PMU) used to estimate the synchrophasor measurements is explained. Measurement reporting standard are briefly discussed and several criteria that are used to evaluate the performance of PMU, are introduced. Since the measurements reported by PMU are actually synchrophasor estimates, in this thesis, the term *measurement* is used as an equivalent to the term *estimate*. Moreover, phasor data concentrator and its applications are presented and communication requirements of synchrophasor data are discussed.

2.1 Synchrophasor concept and definition

A sinusoidal signal in power systems is commonly represented as follows:

$$x(t) = A\cos\left(\omega_n t + \phi\right) \tag{2.1}$$

where where A is the magnitude of the sinusoid, $\omega_n = 2\pi f_n$ is the nominal angular frequency with f_n the nominal frequency (50 Hz or 60 Hz) and ϕ is the phase angle.

The value of ϕ is the angular starting point of the sinusoid at $t = 0$ and depends on the time scale. The phasor representation of the sinusoid is:

$$X = \frac{A}{\sqrt{2}}\, e^{j\phi} \tag{2.2}$$

where $\frac{A}{\sqrt{2}}$ is the root mean square (RMS) value of the signal.

The phasor representation is defined regarding to a specific time scale and the constant nominal angular frequency ω_n. Therefore, to have comparable phasors for several signals, the phasor evaluation must be done with the same time scale and nominal frequency.

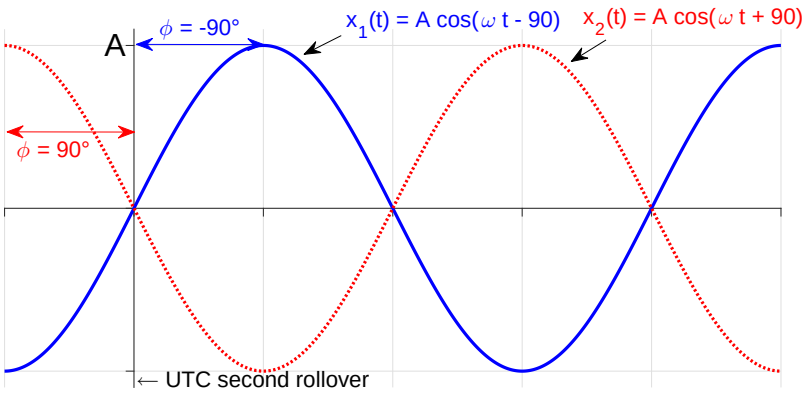

Figure 2.1 Synchrophasor definition for a pure sinusoid at nominal frequency.

The synchrophasor representation of sinusoidal wave $x(t)$ in (2.1) is the same phasor definition in (2.2) where ϕ is measured relatively to a cosine wave with nominal frequency f_n that is synchronized to UTC time reference [45]. The maximum of the reference cosine wave occurs at UTC second rollover (with 1 PPS time signal). By such a definition, ϕ is the phase angle between $x(t)$ and the reference cosine wave. Figure 2.1 shows the concept of the synchrophasor definition. When the positive zero crossing of $x(t)$ happens at UTC second rollover, the synchrophasor angle is $\phi = -90$ degrees. Likewise, when the negative zero

crossing happens at UTC second rollover, the synchrophasor angle is $\phi = 90$ degrees.

In general, a sinusoidal signal has its both magnitude and frequency as functions of time:

$$x(t) = A(t)\cos\left(2\pi \int f(t)dt + \phi\right) \tag{2.3}$$

where $A(t)$ and $f(t)$ are instantaneous magnitude and frequency, respectively, and ϕ is the phase angle.

The voltage and current signals in power system can be expressed as in (2.3). Moreover, a large-scale bulky power system can be considered as a large machine. Therefore, in steady-state conditions, all the generators are rotating at the same speed which means a nearly unique frequency all around the power system. However, this frequency is never constant at its nominal value f_n (60 Hz or 50 Hz). If the total power system demand exceeds total generation, the frequency declines until balance is restored in a new frequency. On the other hand, if the total demand decreases, the frequency increases beyond the target value until the load-resource balance is again achieved. Therefore, the instantaneous frequency of each node can be expressed as the sum of the target frequency and a time-varying deviation term [46]–[50]:

$$f(t) = f_n + \Delta f(t) \tag{2.4}$$

Using the frequency definition in (2.4), the sinusoidal waveform in (2.3) can be rewritten as follows:

$$\begin{aligned} x(t) &= A(t)\cos\left(2\pi \int \Big(f_n + \Delta f(t)\Big)dt + \phi\right) \\ &= A(t)\cos\left(2\pi f_n t + 2\pi \int \Delta f(t)dt + \phi\right) \\ &= A(t)\cos\left(\omega_n t + 2\pi \int \Delta f(t)dt + \phi\right) \end{aligned} \tag{2.5}$$

The synchrophasor representation of $x(t)$ in (2.5) is shown as follows [45]:

$$X(t) = \frac{A(t)}{\sqrt{2}}\, e^{j\left(2\pi \int \Delta f(t)dt + \phi\right)} \tag{2.6}$$

In a special case, where the magnitude is a constant $\frac{A}{\sqrt{2}}$ and Δf is a constant deviation of

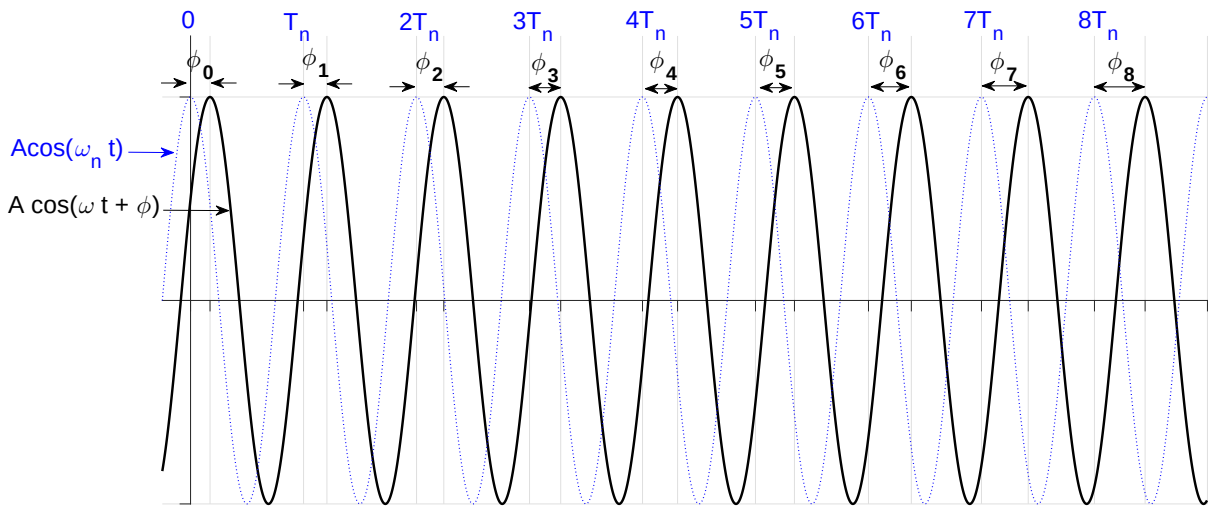

Figure 2.2 Synchrophasor definition for a pure sinusoid at off-nominal frequency when $f < f_n$.

the frequency from its nominal value, the synchrophasor representation is:

$$X(t) = \frac{A}{\sqrt{2}}\, e^{j\left(2\pi\Delta f t + \phi\right)} \tag{2.7}$$

The phase angle of the synchrophasor in (2.7) that is commonly wrapped to the interval $[-180^\circ \;\; 180^\circ]$ is given:

$$\Phi(t) = 2\pi\Delta f t + \phi \tag{2.8}$$

From (2.8), the constant rate of change of the reported phase angle is given [45]:

$$2\pi T_n \Delta f = 2\pi T_n\left(f - f_n\right) \tag{2.9}$$

Figure 2.2 shows the phase angle Φ of the synchrophasor given in (2.7) observed at instants that are T_n seconds apart. The nominal power system period is given by $T_n = 1/f_n$ in seconds. Note that in Figure 2.2, $f < f_n$ results in $\Delta f < 0$ and also $\phi < 0$. Hence, the phase angle Φ changes uniformly over time. Figure 2.3-(a) shows the measured phase angle of an off-nominal frequency sinusoid with $f < f_n$, that decreases uniformly until it reaches -180°, wraps around 180°, and then begins to decrease again. Figure 2.3-(b) depicts the observed phase angle of a sinusoid with $f > f_n$ that constantly increases during the time and wraps around $\pm 180^\circ$.

Based on synchrophasor estimation concept, a precise time reference is needed to provide the UTC time in order to determine the phase angle. Using this method, all synchrophasor

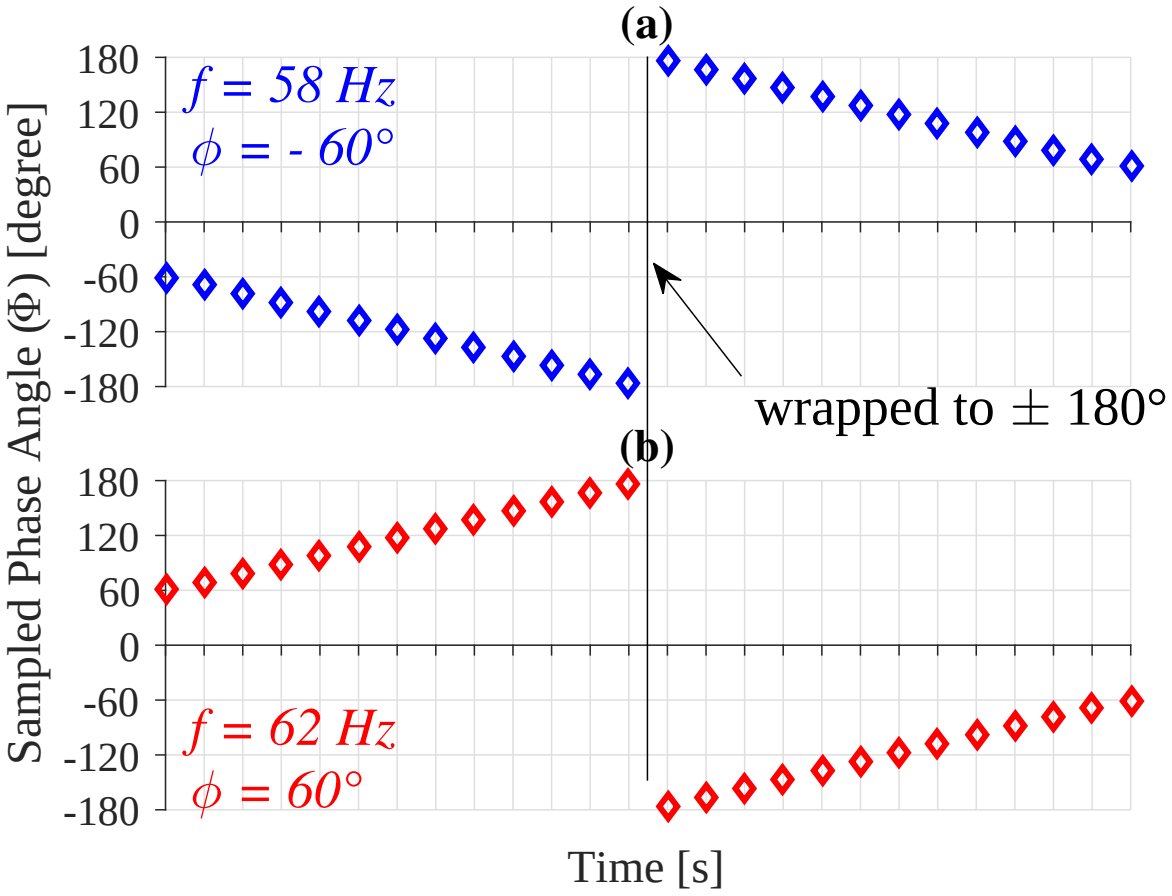

Figure 2.3 Phase angle measurement and sampling for off-nominal sinusoids, (a): $f < f_n$ and (b): $f > f_n$.

measurements are based on a common nominal frequency and time reference, and thus, are comparable. Synchrophasor measurements are variables of time and are effected by the power system oscillations and frequency swings.

2.2 Phasor measurement unit

IEEE Std. C37.118.1 defines the measurement requirements for synchrophasors, frequency and ROCOF in steady-state and dynamic conditions [45]. It also defines the phasor measurement unit (PMU) that is a device capable of estimating and reporting synchrophasors, frequency and ROCOF from voltage and/or current signals. PMU measurements must meet the general definitions and minimum accuracy requirements defined by *IEEE Std. C37.118.1*. A PMU uses a time synchronizing signal to provide comparable synchrophasors with other PMUs. To keep the estimation errors within the limits, PMU must be capable of receiving

time from a reliable time source that is accurate enough to establish traceability to UTC. The device must provide real-time output stream that conforms to the standard requirements.

2.2.1 PMU measurements and structure

The PMU should be capable of estimating and reporting the values of synchrophasors that are defined in (2.7). Single phase and/or positive sequence synchrophasor estimations should be provided by PMU. The sinusoid definition in (2.5), with $A(t) = A$ and $\Psi(t) \triangleq \Big(\omega_n t + \int \Delta f(t)dt + \phi\Big)$ can be rewritten as:

$$x(t) = A\cos\Big(\Psi(t)\Big) \tag{2.10}$$

Noting that synchrophasors are measured based on nominal frequency f_n, the definition of frequency is then given as [45]:

$$f(t) = \frac{1}{2\pi}\frac{d\Psi(t)}{dt} = f_n + \Delta f(t) \tag{2.11}$$

The ROCOF is defined as [45]:

$$\text{ROCOF}(t) = \frac{df(t)}{dt} = \frac{d[\Delta f(t)]}{dt} \tag{2.12}$$

In steady-state conditions, where $\Delta f(t) = \Delta f$, the frequency is constant $f(t) = f_n + \Delta f$ and the measured ROCOF is zero.

Figure 2.4 shows the diagram of a single PMU connected to the power grid [23]. The three-phase voltage and current signals are attenuated and then fed to the PMU inputs. Figure 2.5 depicts the block diagram of the structure of a typical PMU. It has the same hardware of a digital recorder except for its synchronizing parts [22]. The three-phase currents and voltages acquired from secondary windings of current and voltage transformers in Figure 2.4 are the analog inputs to anti-aliasing filters of the PMU. Anti-aliasing filters are used to ensure that the relative magnitude and phase angle of three-phase signals remain unchanged. The frequency response of the anti-aliasing filters is determined by the sampling rate of the process.

Analog to digital (A/D) converters are used to digitize the analog AC outputs of the anti-aliasing filters. A phase-lock oscillator clocked by a reference time source (typically a GPS) provides the high-speed synchronized sampling with 1-microsecond accuracy to the A/D converter. Different digital signal processing techniques can be used to estimate synchrophasors,

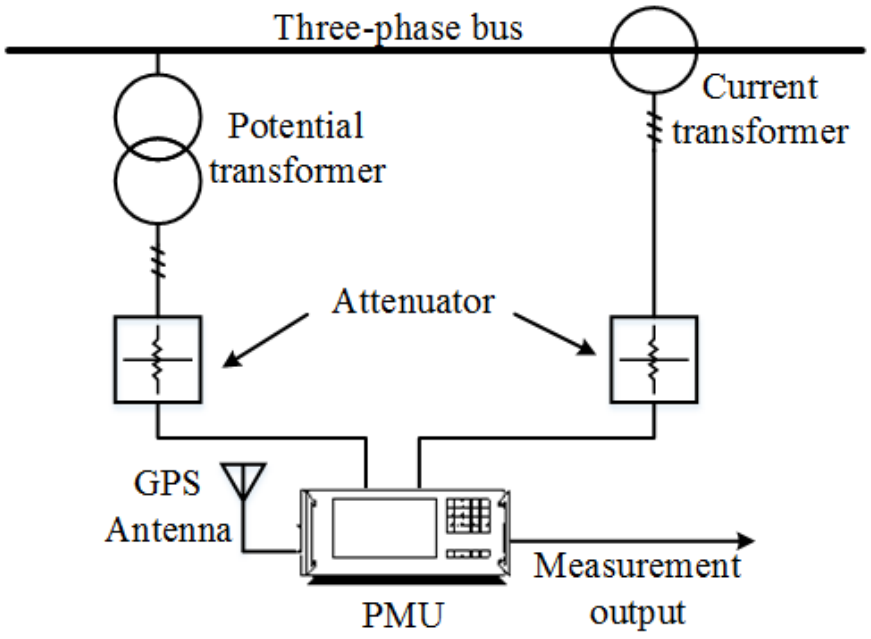

Figure 2.4 Diagram of a single PMU connected to the power grid.

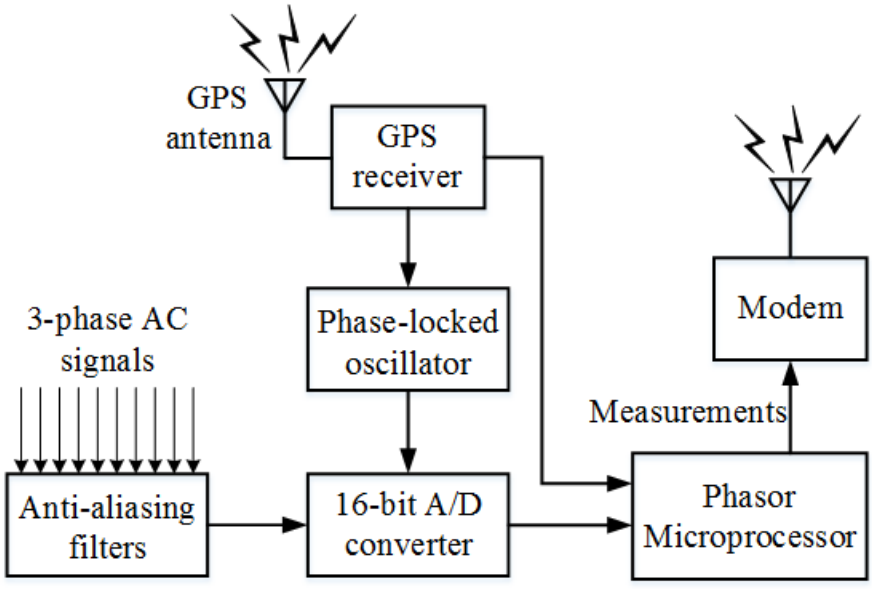

Figure 2.5 Block diagram of the hardware of a typical PMU.

frequency, and ROCOF. Finally, the measurements are communicated to other monitoring or protection devices.

2.2.2 PMU measurement reporting

A set of PMU measurements including synchrophasor, frequency, and ROCOF estimates of a same time instant, that are tagged with a timestamp, is called *data frame*. The data frames should be reported at a constant reporting rate (F_s) and the reporting intervals ($1/F_s$) should be the same. When the number of reported measurements per second is more than one, then the reporting rate should be an integer number of frames per second (fps). With an integer F_s, in each one-second interval there are F_s data frames numbered from 0 to $F_s - 1$ that time spaced equally. The first data frame in each one-second interval should be aligned with the UTC (1 pulse per second) second rollover. This standard of time tagging is under synchrophasor definition in 2.1.

Table 2.1 PMU standard reporting rates

Nominal frequency [Hz]	**60**						**50**		
Reporting rate F_s [fps]	10	12	15	20	30	60	10	25	50

Table 2.1 shows the standard required reporting rates of PMU for power systems with nominal frequencies of 60 Hz and 50 Hz [45]. The required reporting rates are sub-multiples of the nominal frequency. However, higher and lower reporting rates such as 120 fps, 240 fps and 1 fps are permitted to be supported by commercial PMUs. Note that if the reporting intervals are greater than one second, then the reporting rate should be an integer number of seconds between two consecutive data frames (spf).

2.2.3 PMU performance requirements

The standard [45] defines two performance classes for PMU, namely M-class and P-class. The M-class is intended for applications in which the precision is the most important requirement, while the P-class is more suitable for applications with fast measurement time such as protection. The requirements for dynamic performance of these two classes are different. According to the standard [45], a PMU should provide at least one of the two performance classes. The *IEEE Std. C37.118.1* specifies the performance criteria of each class for both steady-state and dynamic conditions. It also provides necessary detailed requirements in several tables to assure that both steady-state and dynamic performances comply with the standard. The manufacturers may choose any estimation methods, algorithms, and hardware as far as their PMUs satisfy the required specifications and tests. In this section, several performance criteria are introduced.

Synchrophasor evaluation

Given a sine wave, the actual synchrophasor representation and the estimate given by PMU may be different in magnitude and phase angle. PMU synchrophasor estimates should maintain both magnitude and phase angle accuracy. Synchrophasor estimation accuracy can be evaluated using the total vector error (TVE). TVE is calculated using the real and imaginary parts of PMU estimates and the actual sample of a synchrophasor. The Polar form of the synchrophasor, given in (2.7), can be converted to the Cartesian form:

$$X(t) = X_r(t) + jX_i(t) \tag{2.13}$$

where $X_r(t)$ and $X_i(t)$ are the exact theoretical real and imaginary parts of the synchrophasor, respectively [45].

The percentage TVE can be calculated for any time instant k:

$$\begin{aligned} \mathrm{TVE}(k) &= 100\frac{\left|X(k) - \hat{X}(k)\right|}{\left|X(k)\right|} \\ &= 100\sqrt{\frac{\left[X_r(k) - \hat{X}_r(k)\right]^2 + \left[X_i(k) - \hat{X}_i(k)\right]^2}{X_r^2(k) + X_i^2(k)}} \end{aligned} \tag{2.14}$$

where $\hat{X}_r$ and $\hat{X}_i$ are the real and imaginary parts of the synchrophasor estimates $\hat{X}$ given by PMU.

Figure 2.6 shows the relationship between the actual synchrophasor, the estimated synchrophasor and a limited TVE. The maximum allowed TVE is given by ϵ, that is depicted as the radius of a circle centered at the end of the vector of the actual synchrophasor. If the end point of the vector of the estimated synchrophasor lies outside the TVE circular region, then the estimate violates the required TVE. On the other hand, any estimate whose end point is encircled by the circle satisfies the required accuracy. The maximum phase angle estimation error with no magnitude estimation error occurs when the estimated synchrophasor is tangent to the circle. The maximum magnitude estimation error with no phase angle estimation error is $\pm\epsilon$.

The TVE is a combination of magnitude and phase angle estimation errors. Therefore, (2.14) can be rewritten as [47]:

$$\mathrm{TVE}(k) = \sqrt{2\Big(1 \pm \lambda(k)\Big)\Big(1 - \cos\gamma(k)\Big) + \lambda(k)^2} \tag{2.15}$$

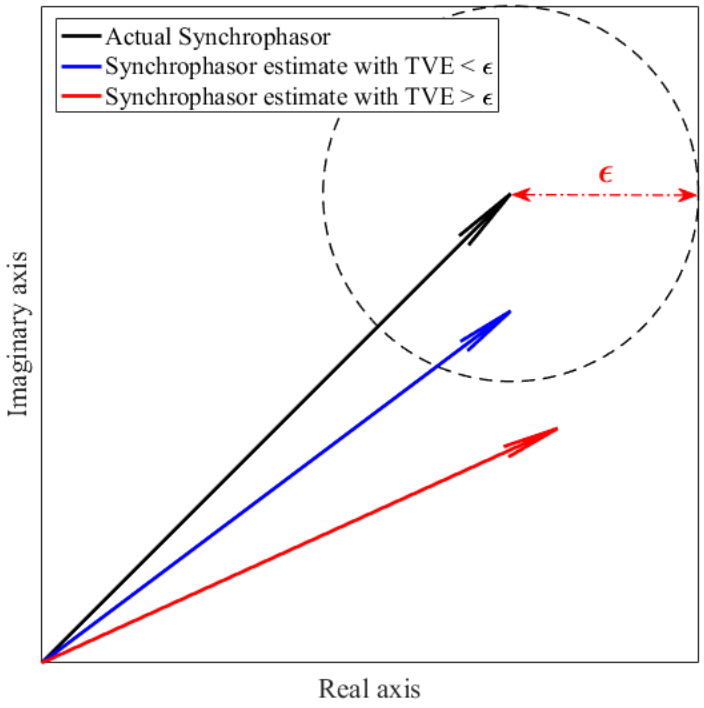

Figure 2.6 The graphical concept of TVE

where $\lambda(k)$ is the magnitude estimation error and $\gamma(k)$ is the phase angle estimation error.

Frequency and ROCOF evaluation

A PMU should also provide frequency and ROCOF with small estimation errors. Both frequency and ROCOF instantaneous estimation errors can be calculated as the absolute value of the difference between the actual and the estimated values [45]:

$$\mathrm{FE}(k) = \left|\hat{f}(k) - f(k)\right| \tag{2.16}$$

$$\mathrm{RFE}(k) = \left|\hat{\mathrm{ROCOF}}(k) - \mathrm{ROCOF}(k)\right| \tag{2.17}$$

where FE and RFE are the frequency measurement error and the ROCOF measurement error, respectively. $f(k)$ and $\mathrm{ROCOF}(k)$ are the actual theoretical frequency and ROCOF, while $\hat{f}(k)$ and $\hat{\mathrm{ROCOF}}(k)$ are the estimated values, respectively.

Table 2.2 Maximum measurement reporting latency for each performance classes

Performance class	**Maximum measurement reporting latency [s]**
M	$5/F_s$
P	$2/F_s$

Measurement delay time and response time

PMU measurement delay time and response time can be evaluated by applying a step change in PMU input (magnitude or phase angle). As a result of the step change in the input, the measurements are disturbed and show a transient response. The measurement delay time is defined as the time difference between the instant of applying the step change and the instant at which the measurement reaches the value equal to the average of the initial input and the steady-state value of the step signal. The measurement response time is defined as the time duration that the estimation errors are greater than TVE, FE and RFE limits.

Measurement reporting latency

PMU's measurement reporting latency is an important factor for fast real-time applications, such as control. Real-time applications (control and protection applications in particular) should consider all reporting delays such as communication delays and measurement latency. Measurement reporting latency is the maximum time difference between the data report time of an event that is indicated by the data frame timestamp and the actual time at which the data frame is available at the output ports of the PMU.

The measurement latency is induced by many factors, such as the estimation and filtering method, processing and reporting time, and the instant within the reporting intervals at which the event occurs. The largest factors are the reporting rate and the estimation method (performance class), while the effect of the relative time difference between the instant at which the event occurs and the reporting time will cause the latency to be greater than one reporting interval ($1/F_s$). The reporting delay is measured for at least 1000 consecutive data frames for any available reporting rate (F_s) and PMU measurement reporting latency is determined as the maximum latency obtained by these tests. Table 2.2 shows the maximum allowed measurement reporting latency for both performance classes [45].

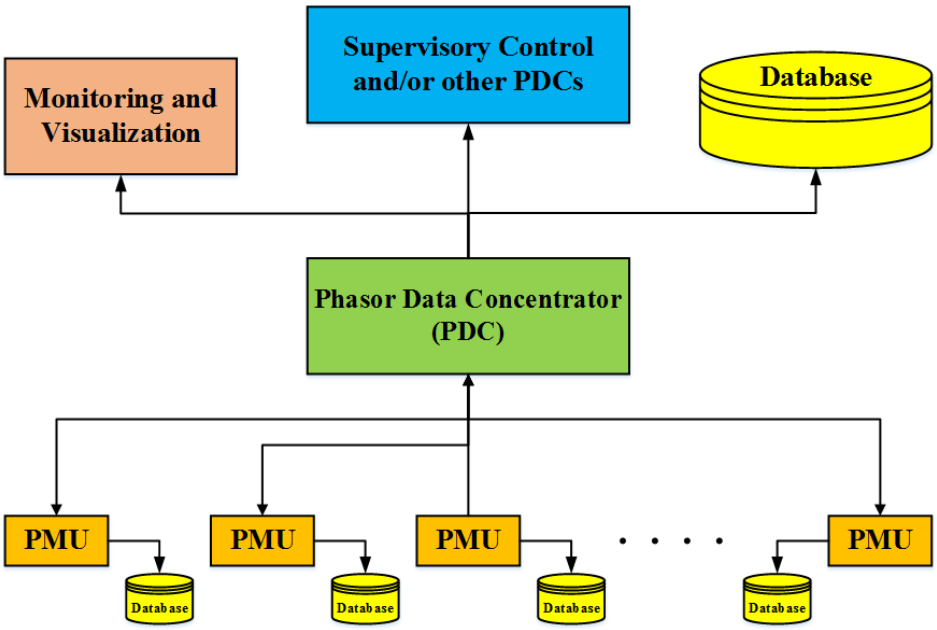

Figure 2.7 Integration of PMU data with a local phasor data concentrator

2.3 Phasor data concentrator

Normally, PMUs are installed in power system substations and generation plants that are remote from each other. At each point of measurement, the PMU data are archived in local storages for future studies. Because of the limited storage capacity, the old measurements will be overwritten by new measurement. Therefore, the important measurements such as the data of a power system event should be flagged for permanent storage. The synchrophasor data can be used either locally or in a remote location from the PMUs. For local applications such as protection and control, the real-time measurements should be available for local controllers and protection units. However, in most cases, the real-time measurements of several PMUs are monitored and processed by a higher level supervisory unit. For such applications, it is necessary to communicate the real-time measurements as a steady data stream.

Figure 2.7 shows a local measurement system consisting of several PMUs, communication links, a local phasor data concentrator (PDC), databases, monitoring units, and supervisory controls [22]. Each PMU has a local storage system that can be accessed locally and from remote locations. The PDC collects data of several PMUs through communication links, discards corrupted data, aligns the data stream of PMUs using their time–stamps, and generates a consistent data stream. The PDC that can be a set of both hardware and software, combines all data from several PMUs having the same timestamp into a single data frame.

Note that the PDC may be recognized as an internal function of a monitoring and control system rather than as a stand-alone device.

Two algorithms can be used by PDC. The first one is a time-based algorithm in which an array of timestamped buffers is used [23]. Data of several PMUs with the same timestamp are grouped together in a single buffer until the data of all PMUs is received and the buffer is full, then the data stream is forwarded to the application. A drawback of this algorithm is that the PDC should wait for all PMUs to send their measurements and that in case of delays the output stream latency is increased. The second algorithm employs a predefined time-out for each timestamped buffer. When the first PMU data of a certain timestamp arrives to the PDC, it is assigned to a new buffer and the countdown to the time-out is initiated. During the time-out, some other PMUs will send their data frames. When the time-out is up, the PDC provides the output data frame without waiting for other PMU data to arrive. The drawback of this algorithm is that the output data of the PDC may be incomplete for certain timestamps. The missing PMU data are called *packet dropouts*.

The communication links between PMUs and the PDC are bidirectional [22]. Most of the data flow are the PMU measurements streaming from the PMU towards the PDC. However, the communication links are also used to send commands to PMUs to change PMU settings and to request specific measurements. A PDC may have an internal database, as well as analytical and mathematical functions that process PMU data. One can benefit the calculating capabilities of the software of a PDC to calculate particular parameters of the power system such as power flow, power losses, power factor, etc. Moreover, by developing analytical and logical functions, the status of certain parts of the power system can be determined. The PMU data can be traced for monitoring and visualization, using external or internal graphical tools.

The real-time, time-aligned data stream of the PDC can be communicated with appropriate speed and latency to supervisory monitoring and control units. For control applications, the latency, that is the time duration between the instant at which the PMU data is created and the instant at which the data is available to the application, is a major factor. For post-event studies, the communication speed and latency is not a key factor.

Another aspect of the communication system is the channel capacity which is the maximum rate at which the data can be transmitted over the communication link. The channel capacity, which is expressed in bits per seconds, depends on the bandwidth of the channel in Hertz, the signal power in Watts and the noise power also in Watts. Therefore, the reporting rate F_s is limited by the available communication channel capacity. However, the PMU data size and rate for most applications is quite moderate and is within the capacity limit of the

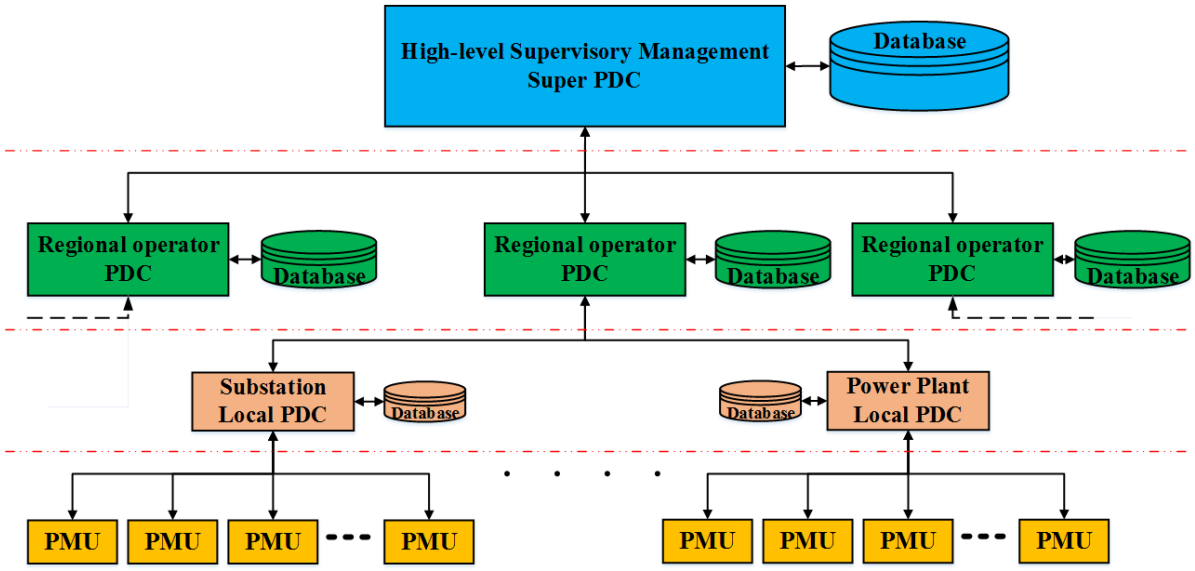

Figure 2.8 WAMS with multi-layer PDC structure.

most communication systems. If the application needs higher PMU reporting rate, then the communication system should have a high channel capacity.

A WAMS consists of multiple PDCs in different hierarchy levels that gather PMU data of a wide area power system and transmit them to the highest supervisory entity. Figure 2.8 shows the typical structure of a WAMS including multiple layers of phasor data concentrating [22]. The lowest level of data concentrating includes PMUs installed in different power plants and substations of a particular region and the local PDCs that concentrate the PMU data of the power plants and substations. The local PDCs may be used for monitoring and data visualization, data analysis and control applications, and protection applications, event detection and alarming. PDCs can use power system measurements such as voltages, currents, and frequency to calculate real and reactive power flows, and other variables and can use them for planning and operating applications.

The second level includes regional PDCs usually located in regional operator stations where the PMU of all the region is concentrated. The PMU data of different power system regions is then transmitted to the highest level of data aggregation system which is usually the power system supervisory management entity. The PDC that is located in the highest level is called super PDC. The super PDC provides real-time synchronized wide area measurements.

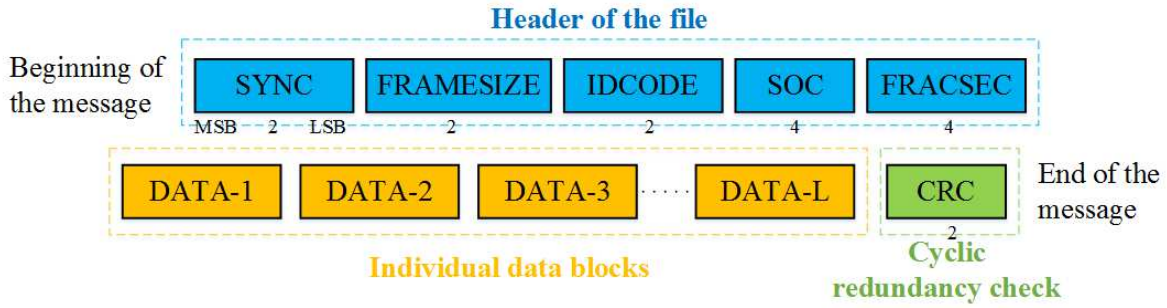

Figure 2.9 Common message format transmitted or received by PMU/PDC.

2.4 Synchrophasor data transfer and message framework

The *IEEE Std. C37.118.2* defines four message types for the configuration and data transmission of PMU or PDC data [51]. These message types are data files, configuration files, header files, and command files. The first three file types are used to transfer data from PMU or PDC to other devices, while the command file is generated by a data receiver device (such as PDC) and is sent to a PMU or a PDC to control the data stream or to request data. The data files communicate PMU measurements to the receiver in a fixed machine-readable format. The configuration files carry the necessary information useful for the interpretation of the data files (e.g. channel numbers, scaling, *TIME_BASE*, etc.) in a machine-readable format. The header files share configuration or descriptive information in a human-readable format with the user of the data. Command files are machine-readable and sent to the PMU or PDC to control the data flow, to change PMU or PDC configuration, and to request current configuration. The *IEEE Std. C37.118.2* defines the configuration and contents of each data file including frame synchronization and checksum. Detailed information can be found in the appendices of *IEEE Std. C37.118.2*.

2.4.1 Common message structure

Figure 2.9 shows the common structure of PMU/PDC output files with three basic sections (header, data blocks, and checksum section). These three sections are defined and explained in the following [51].

Header of the file

Each file frame begins with a header section that has five words. The length of each word in bytes is indicated below the same word in Figure 2.9. The first word (*SYNC*) is used for

synchronization of the transferred data and frame type identification code. The second word (*FRAMESIZE*) carries the total number of bytes in the frame. The third word (*IDCODE*) carries the unique ID number of the PMU/PDC that is the receiver of the command file or the sender of the data, the configuration, or the header file. The next two words that are the second-of-century (*SOC*) and the fraction-of-a-second (*FRACSEC*) provide the exact UTC-based time at which the measurements are reported or the command file is sent. The *SOC* is a four-bytes word containing the number of seconds passed from UTC midnight (00:00:00) of January 1, 1970, to the present second. Each second is divided into a specified number of equally time-spanned fractions. The number of equal fractions in a second is defined by *TIME_BASE* that is given in the configuration file. The four-bytes *FRACSEC* word indicates the number of fractions of a second that are passed from the UTC one-second rollover. The exact time of measurement or transmission is given as follows:

$$UTC\ \ Time = SOC + \frac{FRACSEC}{TIME\_BASE} \tag{2.18}$$

Data section

The data section, which follows the header section, includes several data words, each containing the principal information of a particular PMU, that should be transmitted to or from a PMU/PDC. The number of data words and their length depends on the specifications defined in the configuration file. More information on data word structure is given in 2.4.2.

Checksum section

The last word of any frame is a two-bytes checksum word that is a 16-bit cyclic redundancy check (CRC) computed using the generating polynomial $X^{16} + X^{12} + X^5 + 1$, with initial value of -1 (hex $FFFF$) and no final mask. The check word is used to confirm the data frame validity and to find any errors in data transmission.

2.4.2 Synchrophasor message types

Data frame

Figure 2.10 depicts the block diagram of data frame message format [51]. The data frame contains the measurements and the calculations of the PMU/PDC that are meant to be sent to another PDC. The message begins with the common header section described in 2.4.1. The header section carries the message type ID, message length, the ID of the source of the message, and the timestamp of the measurements. The next section includes multiple

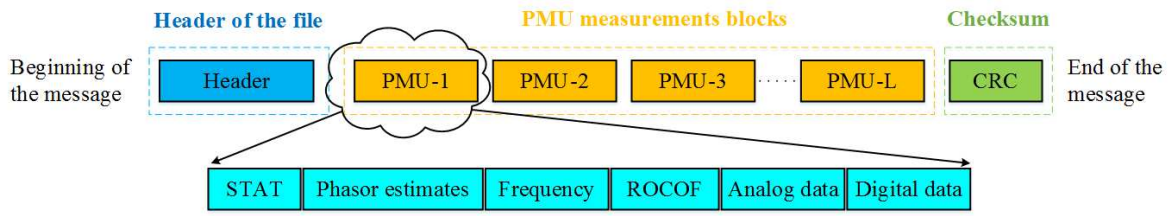

Figure 2.10 Data frame message format.

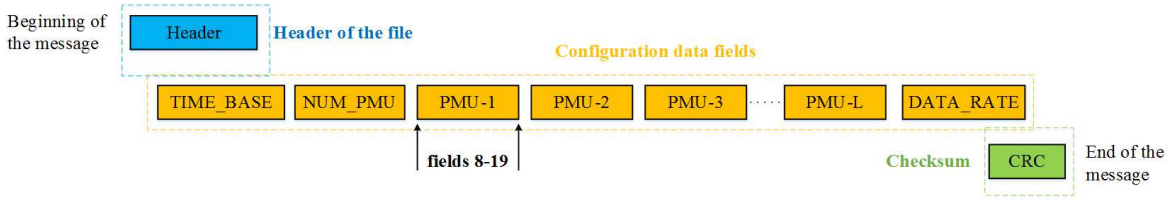

Figure 2.11 The structure of configuration frames *CFG-1* and *CFG-2*.

PMU data words, each containing the data of a single PMU. This allows the transmission of synchronized data from several PMUs corresponding to a unique timestamp. Each data word starts with a status header (*STAT*) and holds phasor measurements, frequency, ROCOF, analog outputs, and digital outputs. All data except digital (Boolean) outputs may be expressed in fixed or floating point format. The two-bytes status flag (*STAT*) designates the complete status of the data word it is heading (e. g. data error flag, synchronization error flag, data sorting types, data modified indicator and PMU time quality). STAT contents are interpreted by the PDC or the application that uses the data. Finally, the message ends with the checksum section.

Configuration frame

There are three types of configuration frame [51]. The configuration frame type is identified in the SYNC word of the message. The configuration frame *CFG-1* contains all the data that the PMU or PMUs are capable of producing and reporting. The umber of PMUs (*NUM_PMU*), the resolution of the *FRACSEC* timestamp (*TIME_BASE*), and the rate of data transmission are among the information that can be found in *CFG-1*. The capability of each individual PMU (e.g. the name of the station or the device, the source's ID code, the data format within the data frames, and the number of phasors, analog and digital outputs) are included in the message frame. Figure 2.11 shows the structure of *CFG-1*. The configuration frame *CFG-2* denotes the measurements currently being transmitted in the data frame. It has the same structure of the *CFG-1* with a fixed frame length of 19 fields

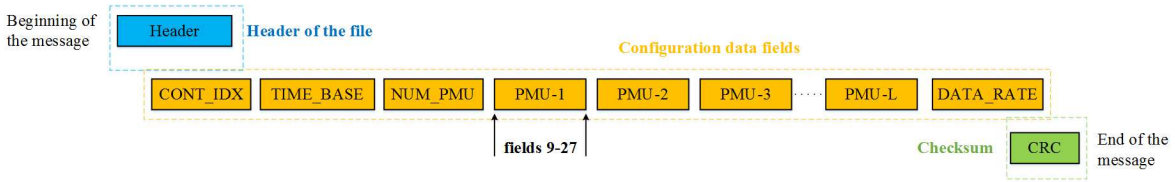

Figure 2.12 The structure of the configuration frame *CFG-3*.

(excluding the rate of the data and checksum). Fields 8-19 define the included measurements from each PMU and can be repeated to cover all PMUs in the message (see Figure 2.11).

The configuration frame *CFG-3* is an optional configuration data frame that has a similar purpose as *CFG-2* and provides the measurements currently being reported in data frames. However, *CFG-3* provides additional information such as the multiplier and the offset values for phasor and analog scaling, the location of PMU (latitude, longitude, and elevation), PMU performance class, and algorithm factors. *CFG-3* has a variable frame length of 29 fields, with fields 9–27 repeated for each single PMU which data are included in the data frame. The variable length of the frame enables a more efficient data transmission (see Figure 2.12). A continuation index for fragmented frames (*CONT_IDX*) has been added to the frame structure of CFG-2. Therefore, large configuration frames can be sent in multiple configuration message fragments.

Header frame

The header frame is used to send human-readable information of the sender (PMU/PDC) to the receiver (normally a PDC). The header message begins with the standard header fields of the general structure (Figure 2.9), continues with a data section in plain ASCII format that contains the human-readable information of PMUs and has no fixed format, and ends with the checksum section.

Command frame

A sending device that can be a PMU or a PDC should be able to send command frames to other PMU/PDC devices to make them start or stop transmission, or to request information in configuration or header frame formats. The command message has the same header and check sections. The command receiving PMU/PDC should identify the authorized sender using the IDCODE before executing the command. The IDCODE also indicates the exact output stream of the command receiving device that is to be configured or changed. Thus, only the selected output stream or streams will change according to the command and the

other streams will remain unchanged. The first field is the two-bytes command word (CMD) and is followed by extended unused words that are reserved for future use. A part of the extended data words can be used to develop user-defined commands.

2.5 *OpenPDC* software

2.5.1 Definition and standards

The OpenPDC operates as a PDC and its main function is to receive the phasor measurements from different PMUs or sources, to time-align them according to the time-tags, and to concentrate them in one or several data streams suitable for storage, real-time applications, or for sending to a PDC in a higher layer of hierarchy [52]. The configuration options in OpenPDC allow the user to collect the synchrophasor data from different sources with different reporting rates and to concentrate them with an arbitrary reporting rate.

The openPDC is a software platform comprised of a complete set of applications for managing synchrophasor data and real-time processing of time-series data streams. The name OpenPDC stands for the open source phasor data concentrator. Currently, the OpenPDC is the most adaptable and flexible phasor data concentrator available. The OpenPDC has a modular design and can be classified as an event stream processor (ESP). The openPDC is a software package designed to comply with all synchrophasor protocols and standards, and to provide user configurable synchrophasor streams.The openPDC is based on the SuperPDC and is developed by the Tennessee Valley Authority (TVA). It was officially launched on 2009. The Grid Protection Alliance (GPA) acquired the development of the openPDC and cooperated with the North American Electric Reliability Corporation (NERC) to expand its use in power systems. Different projects namely TVA.Historian, TVA.PhasorProtocol, and Time Series Framework are combined to develop the OpenPDC [52].

The OpenPDC can execute on Windows service on standard server and workstation hardware for use in substations and also can be used as super PDC in power system management and control services. The OpenPDC is a free license open source software that can be tested in the laboratory and industrial environments prior to any commercial and industrial implementations and commitments. It can be installed anywhere in the synchrophasor phasor data infrastructure. It has been successfully tested on fan-less computers for use in substations.The OpenPDC can support several input protocols including IEEE C37.118, IEEE 1344, IEC 61850-90-5, Macrodyne Versions G and N, SEL Fast Message, BPA PDCstream, and F-NET protocols. Multiple output streams with diffrent configurations can be obtained. A built-in database called openHistorian is available in OpenPDC package that enables the

user to archive the data. A simple web-service call can be assigned to the openHistorian to provide the near-real or the stored data. The OpenPDC's performance statistics including latency, data quality, code errors, and stream statistics for input and output streams are recorded and available every 10 seconds [52].

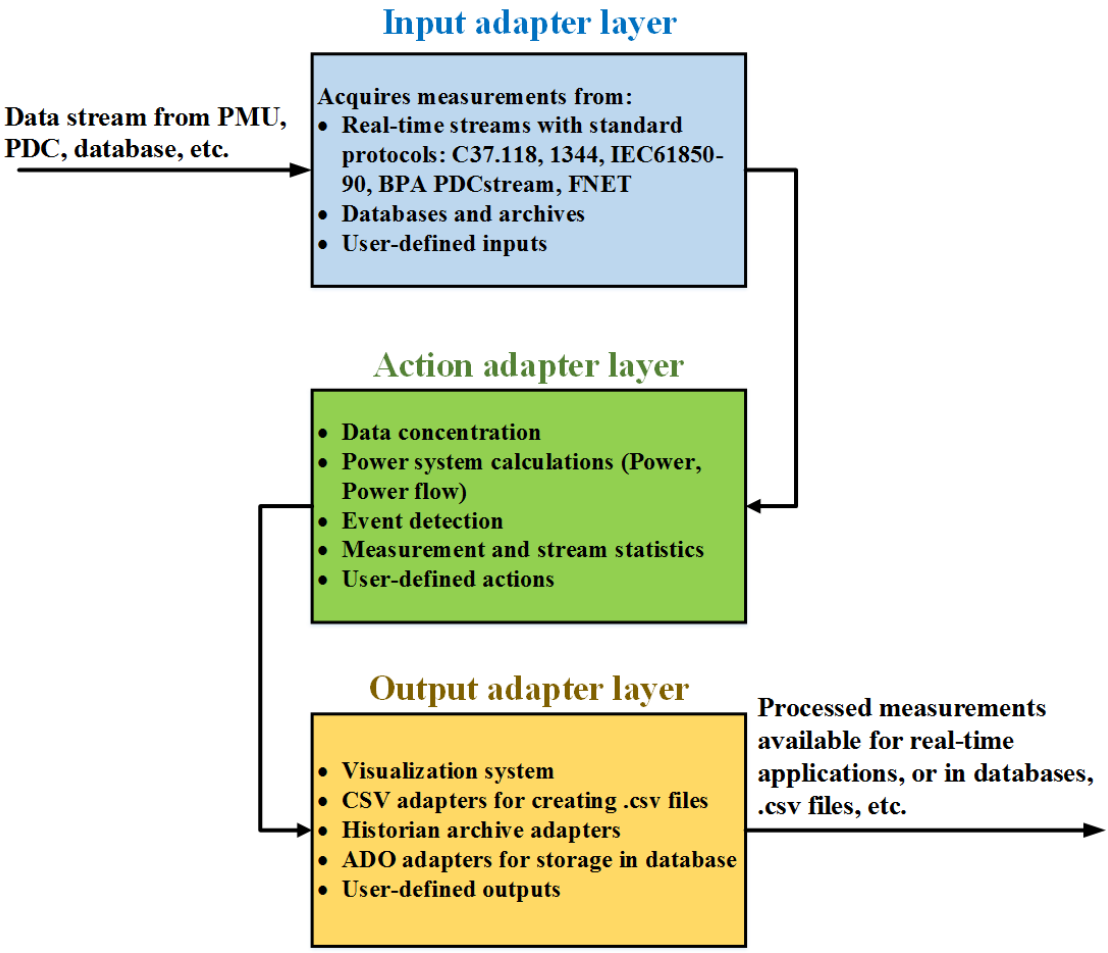

Figure 2.13 The layer structure of OpenPDC

2.5.2 Three-layer structure

OpenPDC is structurally divided into three layers: the input, action, and output adapter layers [52]. As it can be seen in Figure 2.13, Each layer has a particular set of functionalities. The *input adapter layer* is responsible for measurement acquisition from external sources such as PMU and can also introduce new measurements to other adapters. It is capable of parsing and mapping the measurements input streams. The input adapter layer supports different protocols to receive measurements from external devices such as PMU and PDC and makes

the measurements available to the action or the output adapter layers for further processing. Supported communication protocols are IEEE C.37.118, IEEE 1344, BPA PDC Stream, IEC 61850-90-5, and UTK F-Net. To support other communication protocols, customized input adapters can be developed.

The action adapter layer deals with measurement concentrating, sorting, and processing. It can also introduce new measurements to the system like the input adapter layer does. It receives the measurements from the input adapter layer and facilitates the processing of the measurements. Comprehensive mathematical operations, event detection and decision-making processes can be made using PMU data. Several customized calculation action adapters such as power calculator, average frequency calculator, and impedance calculator are available. The calculated measurements can then be sent to the output adapter layer. Moreover, the action adapter layer can be used to implement real-time custom event detection and decision-making algorithms. The analog or digital outputs of such algorithms can be sent to output adapter layer to pass them to other applications or to archive them. The output adapter layer is responsible for measurement routing, data archival, and forwarding tasks. CSV output adapters are used to save the measurements and configurations in .csv format. ADO and MySQL adapters can be used to store data in databases. The output layer can also be used to process and to queue measurements and to stream the measurements using different communication protocols.

2.5.3 Configuration

Figure 2.14 shows a typical configuration of the OpenPDC layers that is useful for measurement archival and real-time applications. This configuration includes three basic types of action adapters that can operate interactively [23], [52]. The sorting adapters are used to sort and concentrate the PMU data of different sources. The processing and calculation adapters facilitate the necessary calculation and event detection. The alarm and statistics adapters are useful to create digital alarm outputs and to produce statistical reports on PMUs and measurement streams. For advanced applications that require processed or secondary measurements, custom action adapters should be included in action layer.

All the functions of input adapters are defined in the *InputAdapterBase* class that is itself defined in the *Time Series Framework* project. Each input adapter requires having access to the information such as IP and port addresses of its corresponding PMU or data stream to extract the synchrophasor data and other configurations. Input adapters specify a unique input measurement key for each input measurement key. The functions of output adapters are defined in the *OutputAdapterBase* class which is also represented in the *Time Series Frame-*

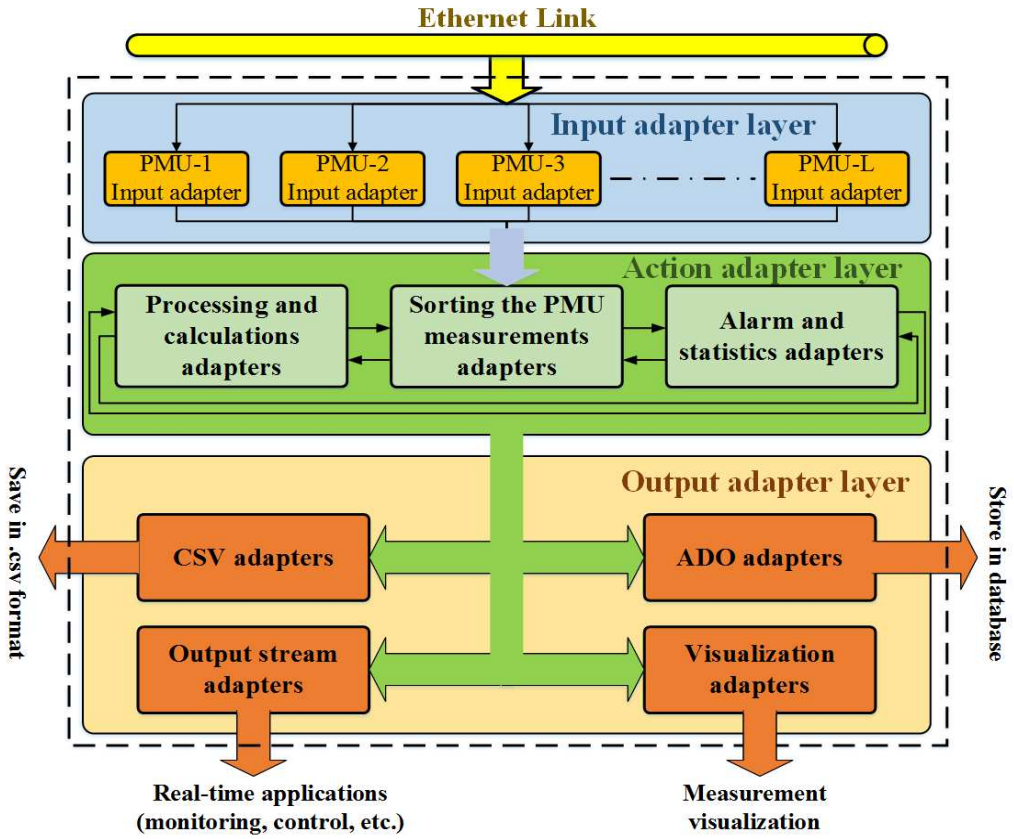

Figure 2.14 A typical configuration of three adapter layers of OpenPDC.

work project. Using the proper output adapter, measurements and data can be stored in a database, saved in a .csv file, or queued as data streams to be sent to real-time applications. A unique measurement key is assigned to each measurement to facilitate its identification.

The OpenPDC consists of various sub-projects. A typical configuration development requires the several elements and conditions. An appropriate *integrated development environment* (IDE) such as Microsoft Visual Studio is required to build and run the openPDC. The openPDC manager employs the *Microsoft .NET 4.0 Framework*. The developer can use an external database such as *Microsoft SQL* or *MySQL* with openPDC. Several sub-projects namely *TVA Code Library*, *Time Series Framework*, *OpenPDC TVA.Historian*, and *OpenPDC Synchrophasor* should be built. The *TVA Code Library* is an open source set of *.NET* codes developed by the *Tennessee Valley Authority* and various open source projects. Most of the internal *.NET* projects of the OpenPDC are developed using the *TVA Code Library* that includes hundreds of class libraries. The *TVA Code Library* provides the necessary standards that make the development and the maintenance of the projects easier. It also improves the speed and reliability of the applications.

CHAPTER 3 ADVANCED PHASOR DATA CONCENTRATOR

In this chapter the structure of the proposed APDC is presented, the LMMSE and the derivative-based estimators are formulated, and the utilized algorithms are thoroughly discussed.

3.1 The proposed APDC

Figure 3.1 shows the general structure of the centralized monitoring scheme using the PDC in smart microgrids. Several PMUs are installed to report the synchrophasor, frequency and ROCOF data at different buses (e.g. the main PCC, local PCs of DERs, and local loads). PMUs transmit their data to the PDC through communication links that are usually imperfect and introduce packet dropouts and delays. The primary task of the PDC is to acquire

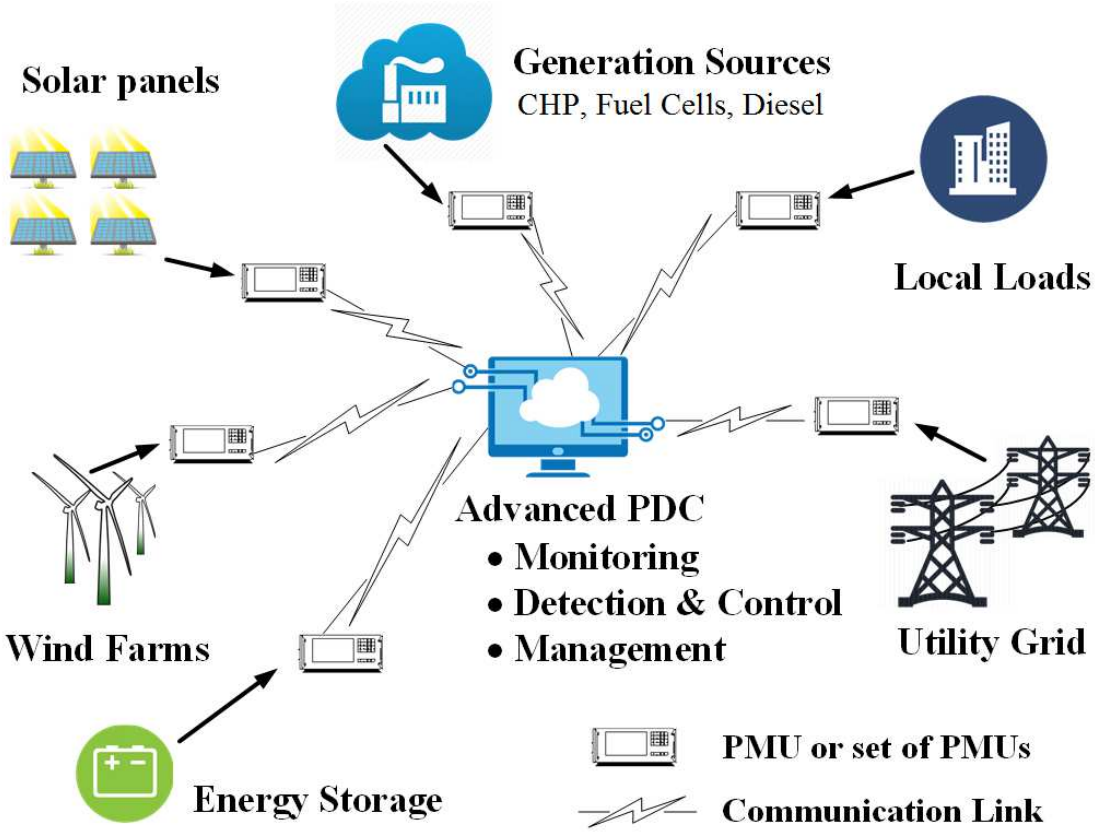

Figure 3.1 The general structure of monitoring, event detection, and microgrid management using APDC [44].

the synchrophasor data frames and provide time-aligned data frames then processes them for certain applications, stores them in local databases, or transmits them to other PDCs or high-level control devices. In a hierarchical control structure, various functionalities can be added to the PDC to enhance monitoring, control, and protection using PMU data. The primary motive to develop the APDC is to process the data sets transmitted over unreliable communication links, to improve monitoring and event detection within the microgrid domain.

Suppose that P PMUs are installed at several distributed nodes of the microgrid, including the PCC, to report the synchrophasor data to a local PDC. The voltage/current signal $x_i(t)$ measured at the i^{th} node, $0 \leq i \leq P-1$, can be expressed as:

$$x_i(t) = A_i(t)\cos\left(2\pi \int f_i(t)dt + \phi_i\right), \tag{3.1}$$

where $A_i(t)$, $f_i(t)$, and ϕ_i are the instantaneous magnitude, frequency, and phase angle, respectively. In this thesis, the node index $i = 0$ is associated with the main PCC as a convention.

The main grid is considered a large and bulky power system or an interconnection in which all the generators are pulling tandem with each other to supply the power demand of the customers. In this case, all the generator units rotate at the same speed and must be near-synchronized at steady-state. The speed of the rotating generators measured in cycles per second or Hertz is the frequency and this implies that a nearly unique frequency is observed at the grid side, and hence, the frequency of the microgrid in the grid-connected mode is imposed by the main grid. However, this frequency does not remain at its nominal value, denoted by f_n (60 Hz in North America). If the total power demand of the loads exceeds the total power generation, then the frequency of the grid declines until the power balance is achieved at a new frequency lower than the nominal frequency. Contrarily, if the total demand of the grid drops lower than the total generation, then the frequency exceeds the nominal value until the energy balance is restored at a new frequency higher than the nominal frequency.

The energy balance is first restored by automatically changing the output of the generators using governors that are sensitive to frequency change and also due to the nature of the power system loads that vary with the frequency. The power demand of some power system loads such as motors is proportional to the frequency of the voltage they are supplied with. Therefore, if the frequency of the grid increases, the power demand of some loads increases. Furthermore, a decrease in the frequency causes the decline of power demand that helps increasing the frequency. This phenomenon helps to restore the power balance partially. If

the power load-generation balance is not restored due to those mentioned above, the Balancing Authorities dispatch generators in a way that each generator can fulfill its individual requirements. The Balancing Authorities can also constrain the amount of the load of the power system by load shedding to sustain the load–generation balance.

Under normal operation conditions, since the load-generation balance is not always achieved, power system frequency slightly fluctuates around the nominal value (f_n). Therefore, the instantaneous frequency at each node can be formulated as the sum of the nominal frequency and a time-varying deviation term as [47] –[49]:

$$f_i(t) = f_n + \Delta f_i(t) \tag{3.2}$$

where $\Delta f_i(t)$ is the instantaneous frequency deviation at the i^{th} node. Hence, Equation (3.1) can be rewritten as:

$$\begin{aligned} x_i(t) &= A_i(t)\cos\Big(2\pi f_n t + [2\pi \int \Delta f_i(t)dt + \phi_i]\Big) \\ &= A_i(t)\cos\Big(2\pi f_n t + \theta_i(t)\Big) \end{aligned} \tag{3.3}$$

The time domain sinusoid in (3.3) can be expressed in the form of a synchrophasor:

$$X_i(t) = \frac{A_i(t)}{\sqrt{2}} e^{j\theta_i(t)} \tag{3.4}$$

where $\theta_i(t)$ is the instantaneous phase angle of the i^{th} node that is synchronized to the UTC.

Figure 3.2 illustrates the fundamental components of the proposed APDC. The APDC includes a conventional PDC that is equipped with an estimation/compensation unit and a monitoring/detection unit. Each PMU reports its measured data frames to the APDC through communication links and data buses. The conventional PDC collects data frames and provides a standard time-aligned output data stream. Then, the estimation/compensation unit processes data sets and, if necessary, compensates for packet dropouts and delays. The compensated data frames are then transmitted to the monitoring/detection unit that continually monitors events by detecting any abnormal changes in voltage/frequency in the microgrid.

Both estimation/compensation and monitoring/detection units are developed inside the APDC. Therefore, the APDC enables fast and reliable event monitoring by avoiding unnecessary data transmissions. The primary objective of the estimation/compensation unit is to provide the monitoring/detection unit with uniform and reliable synchrophasor data frames. Events

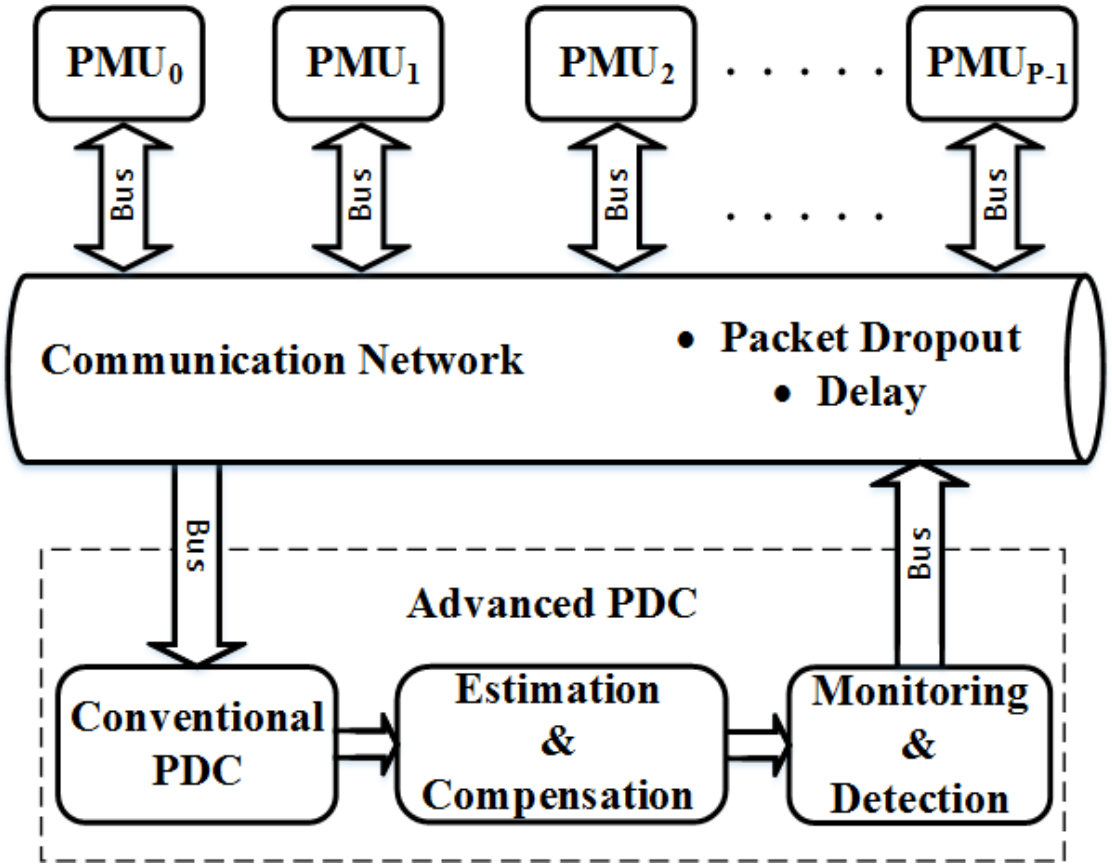

Figure 3.2 Fundamental components of the proposed APDC [44].

that are detected by the monitoring/detection unit are used to enable applications such as microgrid protection, control, and energy management [53].

3.2 Parameter estimation and compensation unit

The purpose of the estimation/compensation unit is to compensate for communication losses and delays to provide the monitoring/detection unit with consistent and reliable data. The main idea for designing the estimation/compensation unit is to continuously estimate the future values of parameters and use these estimates in the case of any communication loss or excessive delays. An estimation method deals with predicting the values of parameters employing the measured data that include a random component. In this work, two methods are considered in the design of the estimation/compensation unit, i.e., a linear parameter estimator and a derivative-based estimator. If there are packet dropouts, lengthy delays, and PMU failures, the estimation methods can predict the value of the parameters using the previously reported data frames.

3.2.1 The linear minimum mean square error (LMMSE) estimator

The linear estimator used in this thesis is the *linear minimum mean square error (LMMSE)* estimator [54]. The estimations rely on the spatio-temporal correlations between data elements of the same type (voltage, current, or frequency) reported by various PMUs at different time instants. Since the data elements of the same type of multiple PMUs are to be estimated, the vector LMMSE that is an extension of the scalar LMMSE is utilized. The goal is to find the linear estimator that minimizes the Bayesian mean square error (MSE) for all data elements of the same type [54].

Assume a scalar parameter $x[N]$ to be estimated based on a data set in the vector form of

$$\mathbf{x} = \begin{bmatrix} x[0] \\ x[1] \\ \vdots \\ x[N-1] \end{bmatrix} \tag{3.5}$$

In this method, the unknown data element $x[N]$ is modeled as a random variable without assuming any particular form for the joint probability density function (PDF) $p(\mathbf{x}, x[N])$. We only need the knowledge of the first two moments to estimate the unknown data element. $x[N]$ can be linearly estimated based on its correlation with $\mathbf{x}$ and the fact that $x[N]$ is statistically dependent on $\mathbf{x}$ as summarized by the joint PDF $p(\mathbf{x}, x[N])$. Considering a LMMSE estimator of the form

$$\hat{x}[N] = \sum_{n=0}^{N-1} a_n x[n] + a_N \tag{3.6}$$

the coefficients a_ns should be selected so they minimize the Bayesian MSE

$$B_{MSE}\Big(\hat{x}[N]\Big) = E\Big[\Big(x[N] - \hat{x}[N]\Big)^2\Big] \tag{3.7}$$

where the expectation $E\Big[(x[N] - \hat{x}[N])^2\Big]$ is with regard to the joint PDF $p(\mathbf{x}, x[N])$ [54]. The coefficient a_N allows nonzero means of $\mathbf{x}$ and if the mean of $\mathbf{x}$ is equal to zero, this coefficient should be set to zero. Note that, a parameter uncorrelated with data set $\mathbf{x}$ cannot be linearly estimated due to the fact that LMMSE relies on the correlation between random elements of the data set.

The optimal value for a_N can be determined by substituting (3.6) in (3.7) and differentiating

the resulting equation and setting it to zero [54]:

$$\begin{aligned}\frac{\partial B_{MSE}\big(\hat{x}[N]\big)}{\partial a_N} &= \frac{\partial}{\partial a_N} E\left[\left(x[N] - \sum_{n=0}^{N-1} a_n x[n] - a_N\right)^2\right] \\ &= -2E\left[x[N] - \sum_{n=0}^{N-1} a_n x[n] - a_N\right] = 0\end{aligned} \tag{3.8}$$

By solving (3.8), the value of a_N is given:

$$a_N = E(x[N]) - \sum_{n=0}^{N-1} a_n E\big(x[n]\big) \tag{3.9}$$

By substituting a_N with the results of (3.9), the Bayesian MSE becomes

$$B_{MSE}\big(\hat{x}[N]\big) = E\left[\left(\sum_{n=0}^{N-1} a_n\Big[x[n] - E\big(x[n]\big)\Big] - \Big[x[N] - E\big(x[N]\big)\Big]\right)^2\right] \tag{3.10}$$

The Bayesian MSE in (3.10) must be minimized over the remaining coefficients a_n. Let

$$\mathbf{a} \triangleq \begin{bmatrix} a_0 \\ a_1 \\ \vdots \\ a_{N-1} \end{bmatrix} \tag{3.11}$$

the (3.10) can be expressed in matrix form

$$\begin{aligned} B_{MSE}\big(\hat{x}[N]\big) &= E\left[\left(\mathbf{a}^T\big[\mathbf{x} - E(\mathbf{x})\big] - \Big[x[N] - E\big(x[N]\big)\Big]\right)^2\right] \\ &= E\Big[\mathbf{a}^T\big(\mathbf{x} - E(\mathbf{x})\big)\big(\mathbf{x} - E(\mathbf{x})\big)^T\mathbf{a}\Big] - E\Big[\mathbf{a}^T\big(\mathbf{x} - E(\mathbf{x})\big)\big(x[N] - E(x[N])\big)\Big] \\ &\quad - E\Big[\big(x[N] - E(x[N])\big)\big(\mathbf{x} - E(\mathbf{x})\big)^T\mathbf{a}\Big] + E\Big[\big(x[N] - E(x[N])\big)^2\Big] \\ &= \mathbf{a}^T\mathbf{C}_{xx}\mathbf{a} - \mathbf{a}^T\mathbf{C}_{x\hat{x}} - \mathbf{C}_{\hat{x}x}\mathbf{a} + \mathbf{C}_{\hat{x}\hat{x}} \end{aligned} \tag{3.12}$$

where $\mathbf{C}_{xx}$ is the $N \times N$ covariance matrix of $\mathbf{x}$, $\mathbf{C}_{\hat{x}\hat{x}}$ is the variance of $\hat{x}$, and $\mathbf{C}_{\hat{x}x}$ is the $1 \times N$ cross-covariance vector with the property of $\mathbf{C}_{\hat{x}x}^T = \mathbf{C}_{x\hat{x}}$. The coefficient vector $\mathbf{a}$ that

minimize (3.10) can be found by differentiating (3.12) and setting the result to zero [54].

$$\frac{\partial B_{MSE}\Big(\hat{x}[N]\Big)}{\partial \mathbf{a}} = 2\mathbf{C}_{xx}\mathbf{a} - 2\mathbf{C}_{x\hat{x}} = 0 \tag{3.13}$$

$$\mathbf{a} = \mathbf{C}_{xx}^{-1}\mathbf{C}_{x\hat{x}} \tag{3.14}$$

By substituting (3.9) and (3.14) in (3.6) the LMMSE estimator is given

$$\begin{aligned} \hat{x}[N] &= \mathbf{a}^T\mathbf{x} + a_N \\ &= \mathbf{C}_{x\hat{x}}^T\mathbf{C}_{xx}^{-1}\mathbf{x} + E\Big(x[N]\Big) - \mathbf{C}_{x\hat{x}}^T\mathbf{C}_{xx}^{-1}E(\mathbf{x}) \\ &= E\Big(x[N]\Big) + \mathbf{C}_{\hat{x}x}\mathbf{C}_{xx}^{-1}\Big[\mathbf{x} - E(\mathbf{x})\Big] \end{aligned} \tag{3.15}$$

and the minimized Bayesian MSE is obtained in close form by replacing (3.14)into (3.12) that is [54]:

$$\begin{aligned} B_{MSE}\Big(\hat{x}[N]\Big) &= \mathbf{C}_{x\hat{x}}^T\mathbf{C}_{xx}^{-1}\mathbf{C}_{xx}\mathbf{C}_{xx}^{-1}\mathbf{C}_{x\hat{x}} - \mathbf{C}_{x\hat{x}}^T\mathbf{C}_{xx}^{-1}\mathbf{C}_{x\hat{x}} - \mathbf{C}_{\hat{x}x}\mathbf{C}_{xx}^{-1}\mathbf{C}_{x\hat{x}} + \mathbf{C}_{\hat{x}\hat{x}} \\ &= \mathbf{C}_{\hat{x}x}\mathbf{C}_{xx}^{-1}\mathbf{C}_{x\hat{x}} - 2\mathbf{C}_{\hat{x}x}\mathbf{C}_{xx}^{-1}\mathbf{C}_{x\hat{x}} + \mathbf{C}_{\hat{x}\hat{x}} \\ &= \mathbf{C}_{\hat{x}\hat{x}} - \mathbf{C}_{\hat{x}x}\mathbf{C}_{xx}^{-1}\mathbf{C}_{x\hat{x}} \end{aligned} \tag{3.16}$$

The LMMSE is suboptimal because it is constrained to be linear [54]. In general, to determine the LMMSE estimator we only need the knowledge of the first two moments of PDF $p(\mathbf{x}, x[N])$ or

$$\begin{bmatrix} E(x[N]) \\ E(\mathbf{x}) \end{bmatrix}, \begin{bmatrix} \mathbf{C}_{\hat{x}\hat{x}} & \mathbf{C}_{\hat{x}x} \\ \mathbf{C}_{x\hat{x}} & \mathbf{C}_{xx} \end{bmatrix}. \tag{3.17}$$

The scalar LMMSE given in (3.15) is suitable for the data output of a single PMU (e.g. voltage, current, or frequency). However, the parameters to be estimated in this thesis are several data elements of the same type obtained from different PMU. The correlation between these parameters allows a more reliable estimation. Hence, the vector LMMSE estimator is employed. The vector LMMSE estimator is an extension of the scalar LMMSE estimator.

Let $x_i[k]$ denote a data element (voltage/current magnitude or frequency) reported by the i^{th} PMU at the k^{th} instant. The last N measurements reported by the i^{th} PMU gives the

data vector $\mathbf{x}_i[k|N]$ defined as [44]:

$$\mathbf{x}_i[k|N] \triangleq \begin{bmatrix} x_i[k+1-N] \\ \vdots \\ x_i[k-1] \\ x_i[k] \end{bmatrix} \tag{3.18}$$

where N is the defined number of data samples that determine the estimation window. Moreover, let $\mathbf{X}[k|N]$ indicate the concatenated data vector formed by accumulating the data vectors of all PMUs [44]:

$$\mathbf{X}[k|N] \triangleq \begin{bmatrix} \mathbf{x}_0[k|N] \\ \mathbf{x}_1[k|N] \\ \vdots \\ \mathbf{x}_{P-1}[k|N] \end{bmatrix} \tag{3.19}$$

where P is the number of PMUs and $\mathbf{x}_0$ denotes the data vector of a single parameter of the main grid. Other PMUs that are reporting the measurements of the microgrid are numbered from 1 to $P-1$.

The concatenated data vector defined in (3.19) contains the last N measurements of the same data type reported by all PMUs. Therefore, for the vector LMMSE estimator to be able to start the estimation process, a complete $\mathbf{X}[k|N]$ vector of last N measurements of all PMUs should be available. Let $\hat{x}_i[k+1|N]$ denote the estimate of data element $x_i[k+1]$ based on the last N data elements reported up to the time instant k. Let the linear estimation be

$$\hat{x}_i[k+1|N] = \sum_{i=0}^{P-1} \sum_{n=k+1-N}^{k} a_{in} x_i[n] + a_{iN} \tag{3.20}$$

We should choose optimal coefficients to minimize the Bayesian MSE with respect to the PDF $p(\mathbf{x}, x_i[k+1|N])$.

$$B_{MSE}\Big(\hat{x}[k+1|N]\Big) = E\Big[\Big(x_i[k+1] - \hat{x}_i[k+1|N]\Big)^2\Big] \tag{3.21}$$

Since P separate estimators are available, the scalar LMMSE estimator can be used for each parameter.

$$\hat{x}_i[k+1|N] = E\Big(x_i[k+1]\Big) + \mathbf{C}_{\hat{x}_i\mathbf{X}}\mathbf{C}_{\mathbf{XX}}^{-1}\Big[\mathbf{X}[k|N] - E(\mathbf{X})\Big] \tag{3.22}$$

where $\mathbf{C}_{\hat{x}_i\mathbf{X}}$ is the $1 \times PN$ cross-covariance matrix and $\mathbf{C}_{\mathbf{XX}}$ is the $PN \times PN$ data-covariance

matrix. The data-covariance matrix is calculated as follows [44]:

$$\mathbf{C_{XX}} = \Big(\mathbf{X} - E\big(\mathbf{X}\big)\Big)\Big(\mathbf{X} - E\big(\mathbf{X}\big)\Big)^T \tag{3.23}$$

By combining the P scalar LMMSE estimator, the vector form of the LMMSE estimator is obtained as

$$\begin{aligned}\begin{bmatrix} \hat{x}_0[k+1|N] \\ \hat{x}_1[k+1|N] \\ \vdots \\ \hat{x}_{P-1}[k+1|N] \end{bmatrix} &= \begin{bmatrix} E\big(x_0[k+1]\big) \\ E\big(x_1[k+1]\big) \\ \vdots \\ E\big(x_{P-1}[k+1]\big) \end{bmatrix} + \begin{bmatrix} \mathbf{C}_{\hat{x}_0\mathbf{X}}\mathbf{C}_{\mathbf{XX}}^{-1}\Big[\mathbf{X}[k|N] - E(\mathbf{X})\Big] \\ \mathbf{C}_{\hat{x}_1\mathbf{X}}\mathbf{C}_{\mathbf{XX}}^{-1}\Big[\mathbf{X}[k|N] - E(\mathbf{X})\Big] \\ \vdots \\ \mathbf{C}_{\hat{x}_{P-1}\mathbf{X}}\mathbf{C}_{\mathbf{XX}}^{-1}\Big[\mathbf{X}[k|N] - E(\mathbf{X})\Big] \end{bmatrix} \\ &= \begin{bmatrix} E\big(x_0[k+1]\big) \\ E\big(x_1[k+1]\big) \\ \vdots \\ E\big(x_{P-1}[k+1]\big) \end{bmatrix} + \begin{bmatrix} \mathbf{C}_{\hat{x}_0\mathbf{X}} \\ \mathbf{C}_{\hat{x}_1\mathbf{X}} \\ \vdots \\ \mathbf{C}_{\hat{x}_{P-1}\mathbf{X}} \end{bmatrix} \mathbf{C}_{\mathbf{XX}}^{-1}\Big[\mathbf{X}[k|N] - E(\mathbf{X})\Big]. \end{aligned} \tag{3.24}$$

Finally, the vector form of LMMSE that gives the one-step-ahead estimates for all data elements is given as [44]:

$$\hat{\mathbf{x}}[k+1|N] = E\big(\mathbf{x}[k+1]\big) + \mathbf{C}_{\hat{\mathbf{x}}\mathbf{X}}\mathbf{C}_{\mathbf{XX}}^{-1}\Big(\mathbf{X}[k|N] - E\big(\mathbf{X}\big)\Big) \tag{3.25}$$

where $\hat{\mathbf{x}}[k+1|N]$ is the $P \times 1$ predicted data vector

$$\hat{\mathbf{x}}[k+1|N] = \begin{bmatrix} \hat{x}_0[k+1|N] \\ \hat{x}_1[k+1|N] \\ \vdots \\ \hat{x}_{P-1}[k+1|N] \end{bmatrix}. \tag{3.26}$$

$E\big(\mathbf{X}\big)$ and $E\big(\mathbf{x}[k+1]\big)$ are the expected values of actual and predicted data vectors, respectively. $\mathbf{C}_{\hat{\mathbf{x}}\mathbf{X}}$ is the $P \times PN$ cross-covariance matrix calculated as follows [44]:

$$\mathbf{C}_{\hat{\mathbf{x}}\mathbf{X}} = \Big(\hat{\mathbf{x}} - E\big(\hat{\mathbf{x}}\big)\Big)\Big(\mathbf{X} - E\big(\mathbf{X}\big)\Big)^T \tag{3.27}$$

The expected values of data vectors in (3.23) and (3.27) are calculated by averaging over a sliding window of archived data.

The LMMSE method provides the minimum estimation error variance to the extent that the variations of input data elements attend a stationary Gaussian distribution. Therefore, the statistics of data do not change over the time. The assumption of Gaussian distribution can be justified through the central limit theorem in non-disturbed conditions given that a large number of consumers contribute to the power demand [55]. In fact, the estimated data vectors calculated from (3.25) have negligible errors when both the main grid and the microgrid are operating in normal conditions (steady-state conditions). However, due to the inherent averaging process in calculations of (3.25), the LMMSE method may exhibit a slow response to sudden changes in the input data. Especially, when the microgrid operates under a disturbed condition (e.g., during islanding events), the voltage/frequency data can vary rapidly in short time intervals. Therefore, under disturbed conditions and during transitions of microgrid between different operation modes, an alternative approach should be used.

3.2.2 The derivative-based estimator

PMUs are capable of calculating and reporting the rate of change of phasor parameters and frequency. Therefore, a feasible alternative is to design and utilize a derivative-based estimator. A derivative-based estimator has a faster response with non-stationary data in disturbed conditions, compared to the LMMSE estimator. A first-order derivative-based estimator can use the present value and the rate of change of data element to estimate the value of the next time instant [44]:

$$\hat{x}_i[k+1] = x_i[k] + \left.\frac{dx_i}{dt}\right|_k \times \frac{1}{F_s} \tag{3.28}$$

where F_s is the reporting rate of PMUs in frames per second (fps). If the data element to be estimated is the frequency, then the ROCOF reported by PMUs is used in (3.28). For other types of data (e.g., voltage and current magnitude), the derivative of the data element can be approximated as its rate of change during two consecutive data frames [44]:

$$\left.\frac{dx_i}{dt}\right|_k \approxeq \Big(x_i[k] - x_i[k-1]\Big)F_s. \tag{3.29}$$

It should be noted that the rate of change of PMU data is highly sensitive to measurement error and noise. Therefore, the estimates obtained from the derivative-based estimator could be relatively inaccurate under normal (non-disturbed) conditions. On the contrary, the esti-

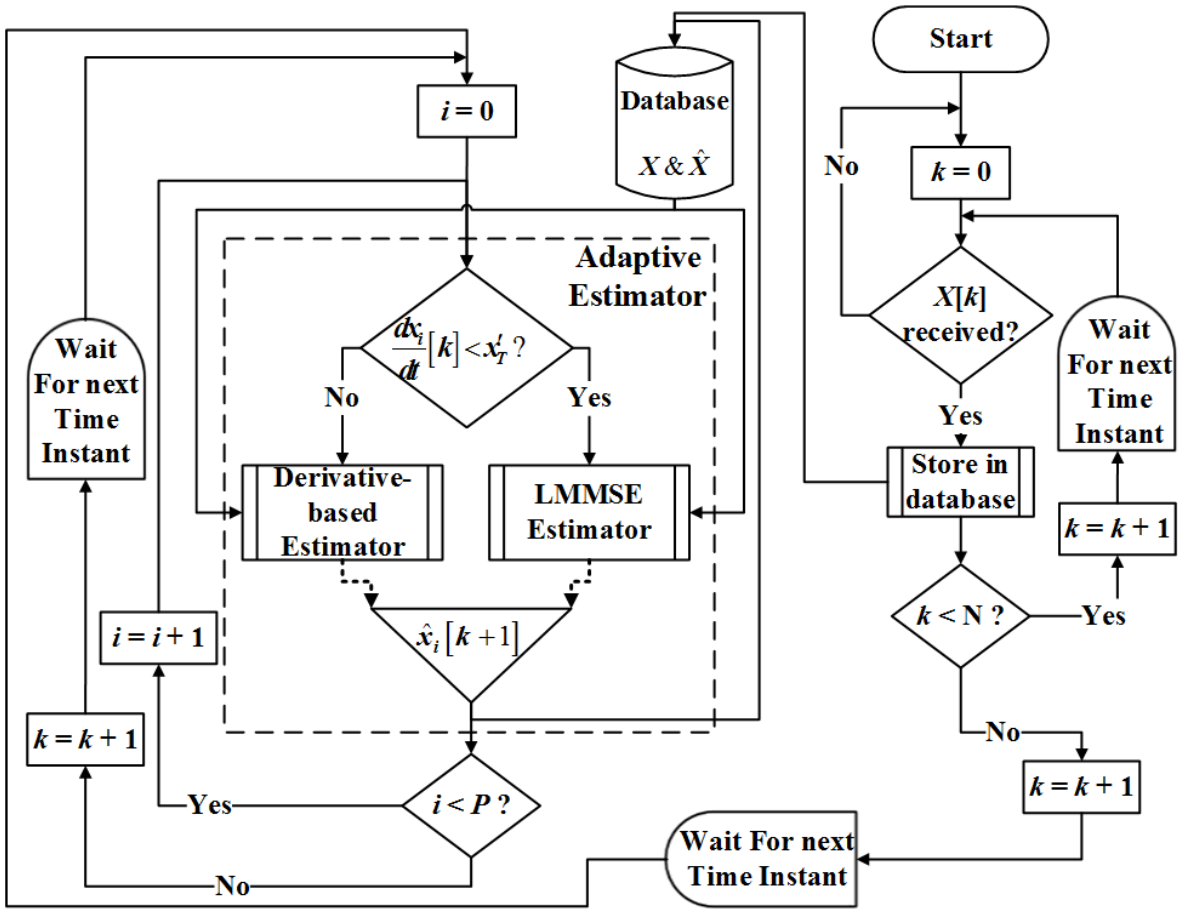

Figure 3.3 Flowchart of the adaptive data estimation/compensation unit of the APDC [44].

mated values based on the LMMSE estimator are more accurate under stationary conditions. Considering the fact that the operational conditions are not *a priori* known, in this work an adaptive data estimator is developed. The proposed adaptive estimator switches between the two estimation algorithms depending on the received data.

3.2.3 The proposed adaptive estimator

Figure 3.3 shows the functional flowchart of the estimation/compensation unit based on the proposed adaptive data estimation approach. At the beginning of the procedure, the unit will collect the data of all PMUs at each time instant, sorts them, and stores them in the database as the concatenated data vectors, X. For initializing, the unit must receive a defined number of N consecutive data of all PMUs without any dropouts or excessive delays. When the number of stored data vectors is equal to N, for each PMU, the estimation is carried out for the data of the next time instant.

At each k^{th} data frame, the rate of change of the data element for the i^{th} PMU is compared with the threshold x'_T. The threshold x'_T is used to distinguish between the normal and disturbed operational conditions of the grid. If a parameter is in normal conditions, then the adaptive estimator must use the LMMSE estimator to estimate the future data elements. On the other hand, If the parameter is disturbed due to an event or a contingency, the adaptive estimator must switch on the derivative-based estimator. Therefore, if the rate of change of parameter is lower than the threshold x'_T (i.e., under normal operation conditions), then the LMMSE estimator is used to predict the data element for the $(k+1)^{th}$ time instant. Otherwise (i.e., during disturbed conditions), the derivative-based estimator is used for estimations. The algorithm repeats the same procedure for all available PMUs. Finally, the estimated values are stored in the same database in a last-in-first-out (LIFO) manner. The algorithm then waits for the data of the next timestamp to arrive. At the $(k+1)^{th}$ time instant, if the PMU measurements are not available, then the stored predicted data elements are retrieved to build the output synchrophasor data set. Therefore, if the data of any PMU at $k+1$ (i.e. $x_i[k+1]$) is not available, the algorithm replaces them with the predicted values stored in the database (i.e. $\hat{x}_i[k+1]$) and continues the estimation process with a complete concatenated data vectors X.

3.3 Monitoring and detection unit

When the compensation of the missing data elements is complete, the monitoring unit processes the synchrophasor data sets and sends event alarms (indicators) as the outputs of the APDC. The event alarms can be used for different applications such as DER islanding detection alarm and protection/control tasks. The primary task of the event detection is to monitor the disturbances in voltage/frequency data continuously.

The frequency excursion detection is a common passive method for islanding detection in microgrids [37], [36]. In the proposed monitoring method, at each time instant, first the magnitude of the frequency error, i.e., $\left|\Delta f_i[k]\right|$, is calculated from (3.2), and then it is compared with a positive threshold, Δf_T. If the frequency error is greater than the threshold, the monitoring unit will reprot a frequency excursion. The value of the threshold affects both the NDZ and the probability of false alarms [35]. Therefore, the monitoring unit must distinguish between a frequency excursion resulted by an actual islanding and those related to load-generation power mismatches. Theoretically, Δf_T must be at least greater than the tight frequency band of power system (e.g. ± 0.06 Hz in North America [56], [57]). Moreover, in practice, Δf_T should be greater enough than the maximum FE of PMUs extracted from the stochastic analysis of frequency data under normal conditions.

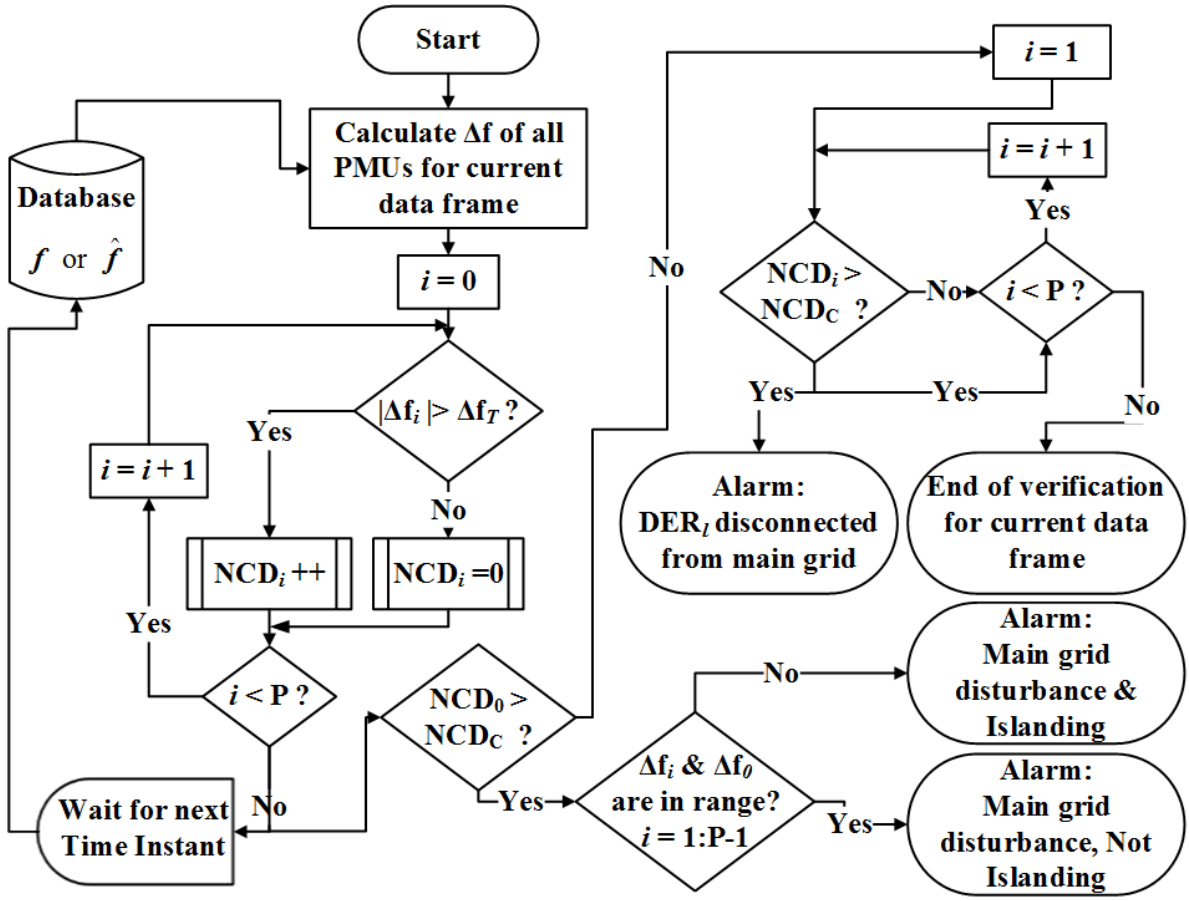

Figure 3.4 Flowchart of DER monitoring by the APDC [44].

Figure 3.4 shows the flowchart of the proposed monitoring algorithm that performs a fast, secure and reliable islanding detection. The synchronized frequency measurements of all DERs and the main grid reported by PMUs are received by the APDC and further processed by the compensation unit. Therefore, we can assume that the frequency estimates of all nodes are always available regardless of packet dropouts and communication delays. At each timestamp, the magnitudes of the frequency error of the main grid, $|\Delta f_0|$, and those of the DERs, $|\Delta f_i|, 1 \leq i \leq P-1$, are calculated and compared with Δf_T. If the frequency of the i^{th} node exceeds the threshold value, then a counter called the number of consecutive detections, NCD_i, is incremented by one. If the frequency error continues to violate the threshold, the NCD_i will increase. When the frequency returns to the acceptable range, the counter resets to zero. Therefore, the value of NCD_i at each time instant can be expressed

as follows [44]:

$$NCD_i[k] = \begin{cases} NCD_i[k-1] + 1, & |\Delta f_i| > \Delta f_T \\ 0, & \text{otherwise} \end{cases} \tag{3.30}$$

If the NCD_i becomes equal or greater than a critical number of consecutive detections, denoted by NCD_c, then a frequency excursion is detected on the i^{th} node and the monitoring unit will alarm the situation. The trade-off between the event detection time and detection reliability depends on the choice of NCD_c. A small NCD_c leads to faster event detection alarms, but it also increases the likelihood of a false alarm due to intermittent perturbations and noise. The designer can determine the best value of NCD_c based on the requirements of the specific application. The NCD_c should be set to 1 to achieve instantaneous event detections. By choosing greater values for NCD_c, the designer can make sure that the islanding detection alarm is reliable and not due to some transient or PMU bad data.

As it is shown in Figure 3.4, at each time instant the algorithm waits for the correspondent frequency data and calculates the NCD_i for $i = 0 : P - 1$ (i.e. for all PMUs available). NCD_0 denotes the number of consecutive detections for the main grid. When all the NCD_i are calculated, the algorithm processes the current time instant information and waits for the frequency data of the next time instant.

As soon as all the parameters NCD_i are updated, the monitoring unit investigates the following four scenarios [44]:

1. $NCD_i < NCD_c$, $\forall i = 0, ..., P - 1$:
   In this case, the number of consecutive detections for the main grid and all DERs is less than its critical value. It means that there are no significant frequency excursions in both the main grid and the microgrid. One can conclude that no islanding event has happened. It should be noted that, depending on the chosen value of NCD_c, there might be actually an islanding event in the process that is not yet confirmed by the monitoring unit.

2. $NCD_0 < NCD_c$ and $NCD_i \geq NCD_c$ for some $i \geq 1$:
   This case indicates that the main grid is operating under normal conditions and shows no frequency excursions while some DER units are experiencing a severe frequency excursion. In this case, one can make sure that the frequencies of the specific DER units are different than that of the main grid. Therefore, the only explanation is that the i^{th} DER is disconnected from the main grid and thus an islanding alarm will be issued for the specified DER units.

3. $NCD_i \geq NCD_c$ and $|\Delta f_i| \approx |\Delta f_0|$, $\forall i = 1, ..., P-1$:
   In this situation, the frequency errors for the main grid and all DERs exceed the normal range. Since the frequency error of all DER units and the main grid are at the same range, one can conclude that the frequency excursion has occurred on the main grid and therefore the microgrid is also affected and shows the same frequency excursion. In this case, one can make sure that the frequency excursion is global and there is no islanding event in the process. Therefore, no islanding alarm will be issued since the entire microgrid is connected to the main grid.

4. $NCD_0 \geq NCD_c$ and $NCD_i \geq NCD_c$, $|\Delta f_i| \neq |\Delta f_0|$ for some $i \geq 1$:
   This case indicates that the main grid and some DER units are suffering from frequency excursion. However, the frequency errors for some DERs are not in the same range with that of the main grid. There is a major frequency disturbance on the main grid while some of the DERs show frequency errors that are not equal to that of the main grid. Therefore, the islanding alarm is issued for potentially isolated DERs.

CHAPTER 4 EXPERIMENTAL SETUP AND RESULTS

In this chapter, the experimental setup implemented using PMUs and OpenPDC software are presented. Moreover, the developed estimation algorithms are evaluated, and the advantages of the proposed adaptive estimator are demonstrated. The performance of the APDC against the islanding events is investigated. Further, the effectiveness of the proposed APDC in the presence of noise is evaluated. Finally, the adaptive estimator is compared with the interpolative estimation method using frequency steady-state and ramp tests.

4.1 Experimental setup

The experimental setup includes 3 VIZIMAX PMUs (that operate according to P class), and the developed APDC that is responsible for monitoring of DERs and their connection/disconnection events [58]. The VIZIMAX PMU employs an adaptive algorithm for robust estimation of synchrophasors. It also employs an efficient filtering against harmonics and noise, and improves the measurement speed up to 20% comparing to the conventional DFT algorithms. The VIZIMAX PMU exceeds the accuracy requirements of the IEEE standard for synchrophasor measurements with the TVE under 0.50% in steady-state conditions. Moreover, the VIZIMAX PMU presents additional communication options including generic object oriented substation events (GOOSE) messaging. The synchronization options with high accuracy clock base of 100 ns are:

- Inter-Range Instrumentation Group time code (IRIG-B).
- The pulse per second (PPS) signals.
- The precision time protocol (PTP).
- The network time protocol (NTP)
- The internal GPS.

The VIZIMAX PMU has an adjustable reporting rate from 1 frame per minute to up to the unique rate of 240 fps for 60 Hz. Joined with the VIZIMAX RightWON^{TM} controller that features a built-in C37.118 client, the VIZIMAX PMU can be used in customized monitoring, control, and protection applications.

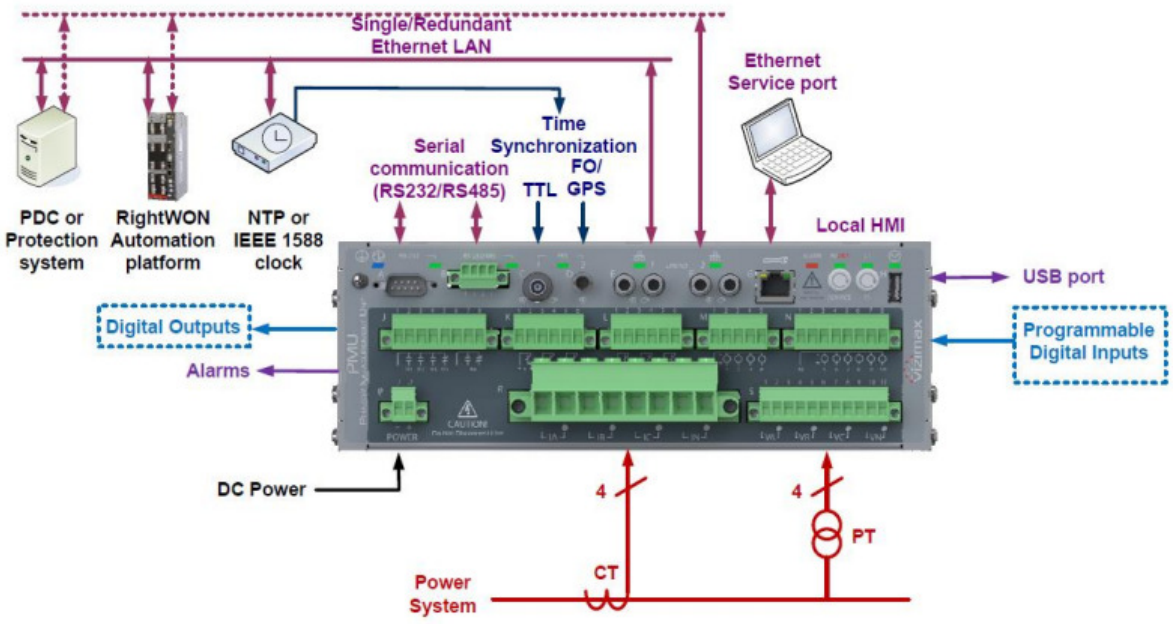

Figure 4.1 The VIZIMAX PMU I/O interface [58].

Figure 4.1 shows the VIZIMAX PMU Input/Output (I/O) interface. The AC voltage/currents acquired from the conventional voltage/current transformers (PTs/CTs) are the input signals that will be converted to synchrophasor and frequency related measurements. The PMU transmits the digital data to an Ethernet LAN using IEEE C37.118 messaging protocol [51]. The PMU has 4 relay outputs for alarming the status of the synchronization and in/out of service. The time synchronization options are as follows:

- IRIG-B synchronization signal received over either fiber optic or the Transistor–Transistor Logic (TTL) port.
- IEC 61588 (IEEE 1588) PTP master clock.
- NTP service enhanced with BNC-TTL or IR fiber PPS inputs.
- Internal GPS clock with high precision PPS output.

Three Ethernet ports are provided for communication of PMU data. Ports 1 and 2 are configurable based on C37.118 and GOOSE messaging protocols. Port 1 is the standard copper Ethernet connection (100BASE-T) with RJ-45 connectors. Port 2 is the fiber-optic connection with two options of either 100BASE-FX with ST type connectors or 100BASE-LX with LC long range. Port 3 is an Ethernet connection used for local service and/or remote maintenance of the PMU and is located on the front panel of the PMU.

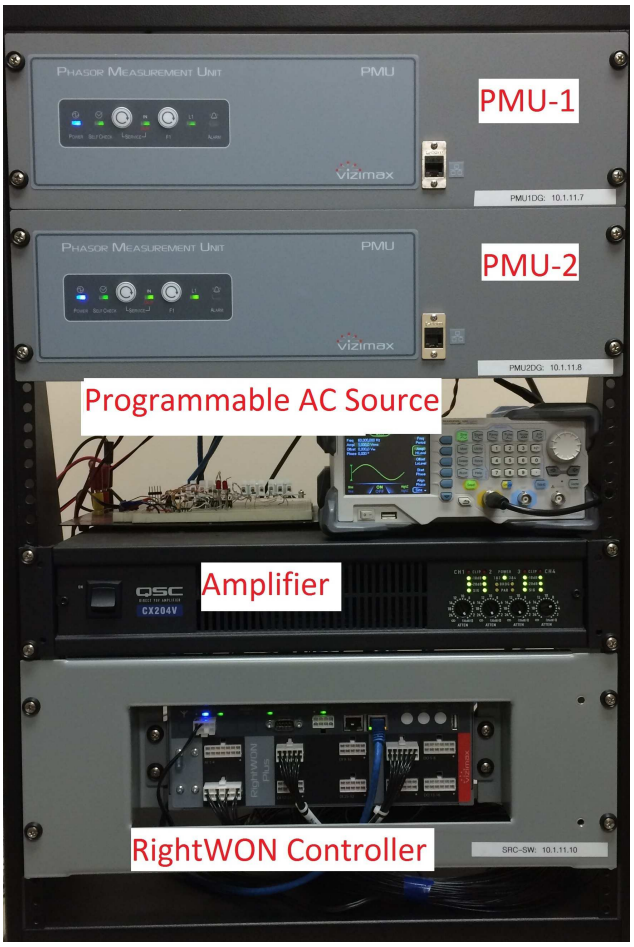

Figure 4.2 Part of the experimental setup including two PMUs, programmable AC source, electrical switch, amplifier and controller [44].

A 48 V DC source is used to power the 3 PMUs. The reporting rate of PMUs is set to $F_s = 60$ fps. One of the PMUs is always measuring the parameters of the *Hydro-Quebec* distribution grid and sends the synchrophasor data frames to the proposed APDC via an Internet connection. The GPS clock is used to synchronize and timestamp the data frames of the *Hydro-Quebec* PMU. Figure 4.2, shows the other two PMUs that are responsible for measuring the voltages/currents at local PCCs of the DERs. The IRIG-B is used for time synchronization which conforms to the requirements imposed by the *IEEE Std. C37.118.2* standard [51]. The synchrophasor data of these two PMUs are transmitted to the APDC through an Ethernet link.

In this thesis, hardware emulation is employed for real-time performance evaluation of the proposed APDC. The transients of the *IEEE 34-bus* network under disturbed conditions (islanding event) is simulated using the Electromagnetic Transients Program (EMTP) [59]. The

Table 4.1 Standard and maximum deviation of frequency and ROCOF measured by PMUs under normal conditions [44].

Param.	Criteria	PMU-0	PMU-1	PMU-2
f [mHz]	Standard deviation	20.456	20.595	20.598
	max $\|\Delta f\|$	96.290	92.980	92.983
ROCOF [Hz/s]	Standard deviation	0.0929	0.1653	0.1654
	max $\|ROCOF\|$	3.6	7.0	7.1

time domain simulation results are then fed to PMUs as input signals using a programmable AC voltage source. The programmable AC voltage source generates the voltage signals at the local PCCs of DERs extracted from simulations. An electrical switch connects the amplified output of the programmable voltage source with the input terminals of the PMUs. In EMTP simulations, the aggregated power generated by the DER units is close to the total demanded power by the loads to the extent on which a slow frequency decrease of 0.5 Hz is observed after islanding of the entire feeder.

All the proposed algorithms are implemented in the *OpenPDC* software [52]. The measurements from the PMUs are transmitted to *OpenPDC* that time-aligns the synchrophasor data. The PMU data are decimated to 40 fps using *OpenPDC* and then delivered to designed action adapters. The action adapters are the developed compensation and detection algorithms capable of real-time data processing. Furthermore, to study the effects of communication impairments, an online packet drop action adapter is developed in the *OpenPDC* platform and employed to perform packet dropout on certain time instants. For given timestamps the data frames of any PMUs can be replaced with Not a Number (NaN) indicator. The corrupted data packets then are sent to the compensation unit.

4.2 Frequency estimation-compensation results

The signals measured by the three PMUs are the voltages of the distribution network. Therefore, the measured frequencies include both load-generation imbalance ($\Delta f_i(t)$ in (3.2)) and noise. When estimating frequency, the threshold x'_T becomes f'_T, which is a limitation on the ROCOF value.

Table 4.1 shows the standard and the maximum deviations of the measured frequency and ROCOF for a period of 30 minutes under normal operation of distribution network. The average standard deviation value for frequency is 20.5 mHz and the maximum frequency deviation from its nominal value is 96.29 mHz (measured by PMU-0 that is located at the

PCC). Although the average of ROCOF is 0 Hz/s over 30 minutes, its average standard deviation is 0.1412 Hz/s with a maximum ROCOF of 7.1 Hz/s (measured by PMU-2 that is located at the PC of the DER-2).

As explained in Section 3.2, the threshold value used for the adaptive estimator is chosen based on two criteria. Firstly, the threshold must be much greater than the average ROCOF standard deviation under normal condition to avoid unnecessary switchings to ROCOF-based estimator. Secondly, it must be small enough to trigger the ROCOF-based estimator if there are frequency excursions. Therefore, under normal conditions and in the presence of noise and frequency deviations, the adaptive estimator principally uses the linear estimator rather than the ROCOF-based estimator. Rigorous studies conducted in this work confirm that with a threshold value of $f'_T = 1$ Hz/s, the ROCOF-based estimator is active at only 0.4 % of the time instants. In general, the value of this threshold depends on the performance and accuracy of PMUs under normal conditions.

Figures 4.3 (a)-(c) show the PMU measured frequencies and those estimated by different estimators under the normal condition. No frequency excursions and/or communication impairments were considered during these tests. The actual frequency on the grid side, f_0, and the actual frequencies at local PCs, f_1 and f_2, present small scale variations principally due to the instantaneous load-generation balance in the *Hydro-Quebec* distribution network. As expected, both LMMSE and ROCOF-based estimation methods follow the actual frequency smoothly. However, the LMMSE estimator has a better accuracy regarding the variance of the estimation error.

Figures 4.4 (a)-(c) show the actual and the estimated frequency data for the PMUs when the entire microgrid becomes islanded from the *Hydro-Quebec* network at time instant $t = 178.55$ s. It can be seen that the LMMSE has a relatively slow response to the frequency excursion, whereas the ROCOF-based estimator exhibits a faster response. Figure 4.4 also shows the results of the proposed adaptive estimator under both normal and disturbed conditions. For the frequency of the main grid f_0, in Figure 4.4 (a), it can be seen that the estimated frequencies using both LMMSE and adaptive estimator are the same during the normal condition. For the DER frequencies, however, when frequency excursion occurs, the APDC switches to the ROCOF-based estimator. In conclusion, the adaptive estimator enables faster and more accurate estimations for missing frequency data.

Table 4.2 confirms the results of Figures 4.3 and 4.4 by comparing the maximum and the average values of FEs extracted from different estimation methods under both normal and disturbed conditions. Here, FE is calculated as the absolute value of the difference between the measured frequency by PMU and those estimated by different estimators. Under nor-

Table 4.2 Performance comparison of different estimation methods under normal and disturbed conditions with unmeasurable noise [44].

Condition	FE	Estimator type		
	[mHz]	LMMSE	ROCOF	Adaptive
Normal	max.	1.8	2.4	1.8
	avg.	0.6	1.1	0.6
Disturbed	max.	388.3	161.4	116.1
	avg.	214.2	61.6	48.9

mal conditions, the maximum and average values of FE of the LMMSE estimator are both less than those of the ROCOF-based estimator. Since the adaptive estimator employs the LMMSE method during normal conditions, the maximum and average values of FE of these

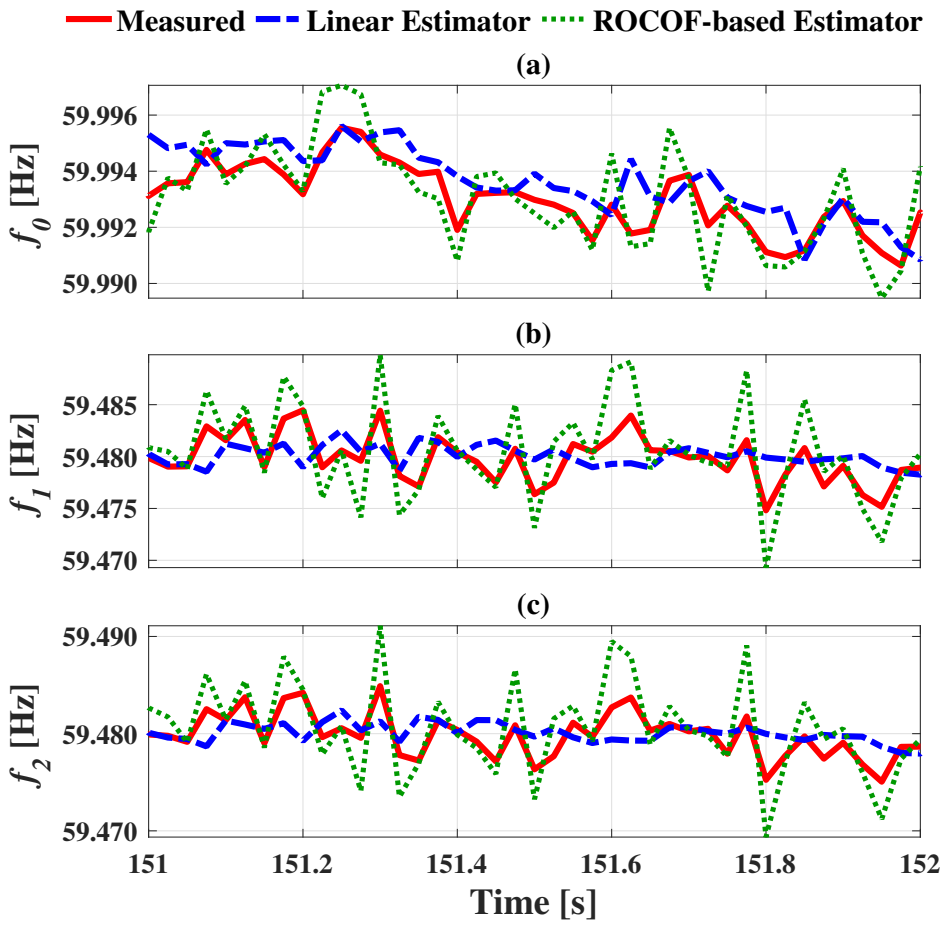

Figure 4.3 Frequency estimation results of different estimators under normal condition: (a) main PCC, (b) DER 1, (c) DER 2 [44].

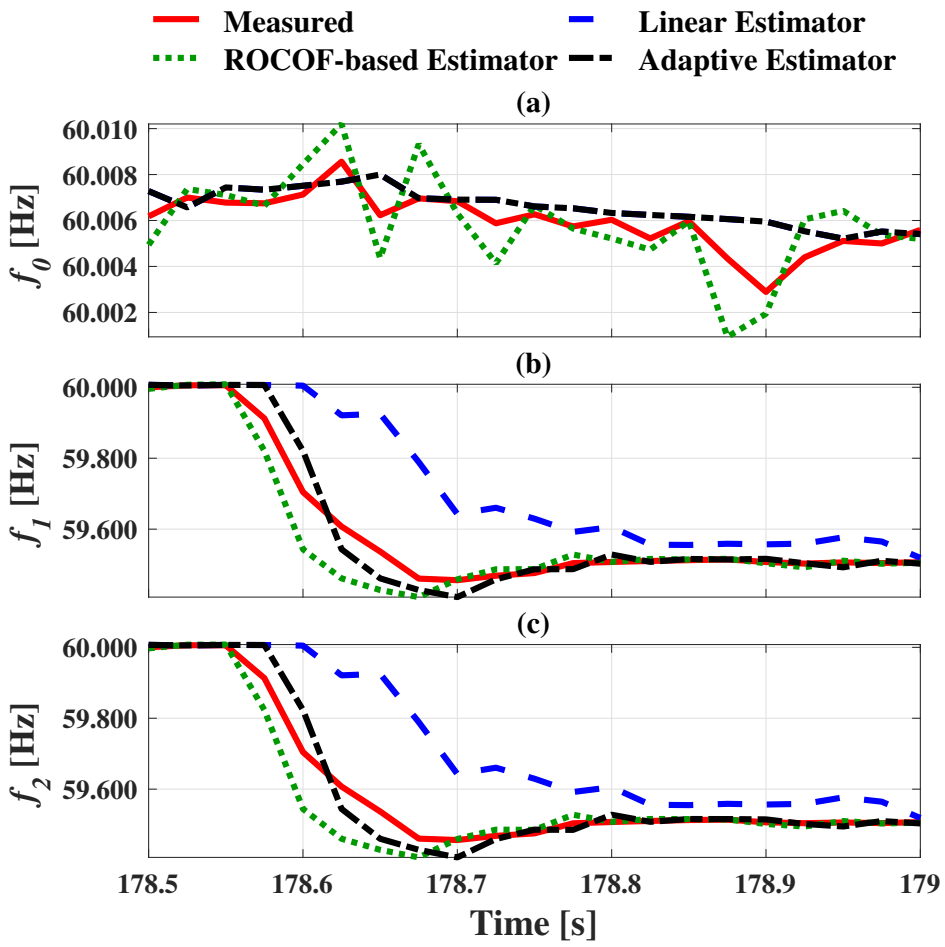

Figure 4.4 Frequency estimation results of different estimators under the disturbed condition: (a) main PCC, (b) DER 1, (c) DER 2 [44].

two estimators are similar. Table 4.2 also reports the results of frequency estimation during an islanding event. The results imply that the maximum and the average values of FE of the LMMSE estimator are higher than those of the ROCOF-based estimator under disturbed conditions. The adaptive estimator, however, switches from the LMMSE to the ROCOF-based estimator that results in a significant improvement of frequency estimation. The maximum FE of the adaptive estimator during the islanding event is calculated 0.0489 Hz that is an acceptable value regarding the frequency step change of 0.5 Hz.

4.3 Islanding detection results

The critical number of consecutive detections and the frequency deviation threshold are set to $NCD_c = 1$ and $\Delta f_T = 0.15$ Hz, respectively. The selected Δf_T is greater than both

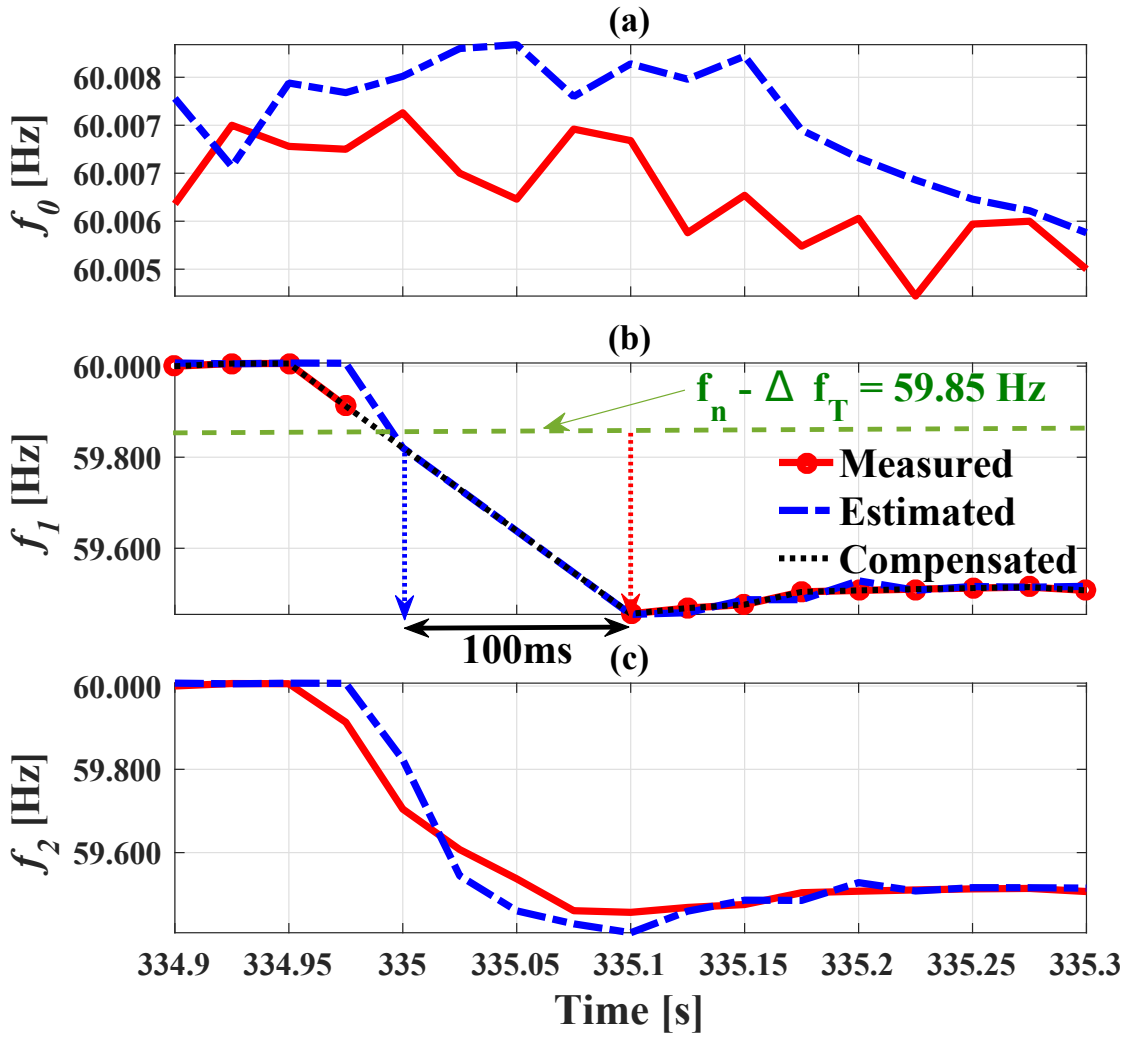

Figure 4.5 Performance of the proposed APDC regarding to islanding detection under successive packet dropouts: (a) frequencies of the main PCC, (b) frequencies of DER 1, (c) frequencies of DER 2 [44].

the North American tight frequency band of 0.06 Hz and the PMU's maximum FE of 0.096 Hz during normal conditions given in Table 4.1 [56], [57]. Hence, the risk of false detection is decreased. Also, the chosen Δf_T is small enough to enable a fast and secure frequency excursion detection. Moreover, the selected value of NCD_c facilitates fast islanding detections with small NDZ. However, to further prevent false alarms the NCD_c can be selected greater than 1.

The two DER units are simultaneously islanded at $t = 334.95$ s to examine the performance of the monitoring unit. Moreover, four data packets from DER_1 are intentionally discarded at exactly two data frame after islanding time, i.e., at $t = 335$ s. Figures 4.5 (a)-(c) show the

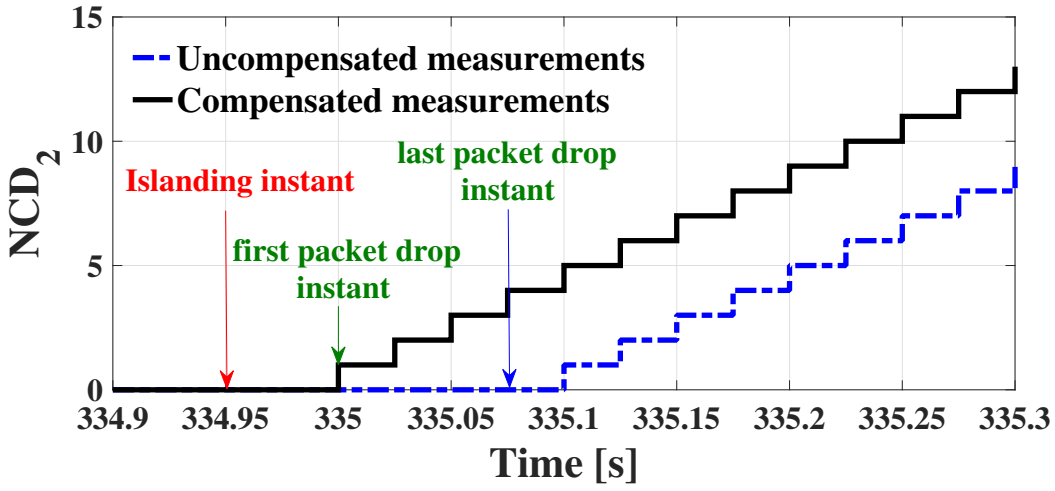

Figure 4.6 The number of consecutive detections for PMU of DER 2 with and without packet dropout compensation [44].

actual frequency data including the packet dropouts on the output of PMU 1, the estimated frequencies, and the compensated data of f_1. The estimated frequency is used only when the PMU frequency data are not available. As soon as the frequency exceeds the critical value, $f_n - \Delta f_T = 59.85$ Hz, and before any data reported by PMUs are available, four consecutive packet dropouts occur for PMU 1. If there is no frequency estimation/compensation, then the first possible islanding detection would be at $t = 335.1$ s. i.e., 5 data frames later. This means a detection delay equal to four sampling times, i.e., 100 ms. However, utilizing the compensation unit, all the missing data are replaced by the estimated values. This provides the detection algorithm with consistent frequency data, as shown by the dashed line in Figure 4.5 (b).

Figure 4.6 shows the number of consecutive detections during the islanding detection process. If the compensation unit is not employed, the parameter NCD_2 will remain 0 during the packet dropouts and only equals 1 at $t = 335.1$ s where the first PMU data frame arrives. By using the compensation unit, the parameter NCD_2 increases to 1 at the same frame where the first packet dropout occurs ($t = 335$ s). Therefore, the APDC enables a 100 ms faster islanding detection comparing to the frequency excursion methods that use uncompensated PMU data. The results in Figures 4.5 and 4.6 confirm the advantages of using the proposed APDC for time-critical monitoring applications with communication impairments.

Figures 4.7 (a)-(c) show the actual frequency data including the packet dropouts on the output of PMU 1 and PMU 2, the estimated frequencies, and the compensated data of f_1 and f_2. The two DER units are simultaneously islanded at $t = 173.425$ s. Four data packets

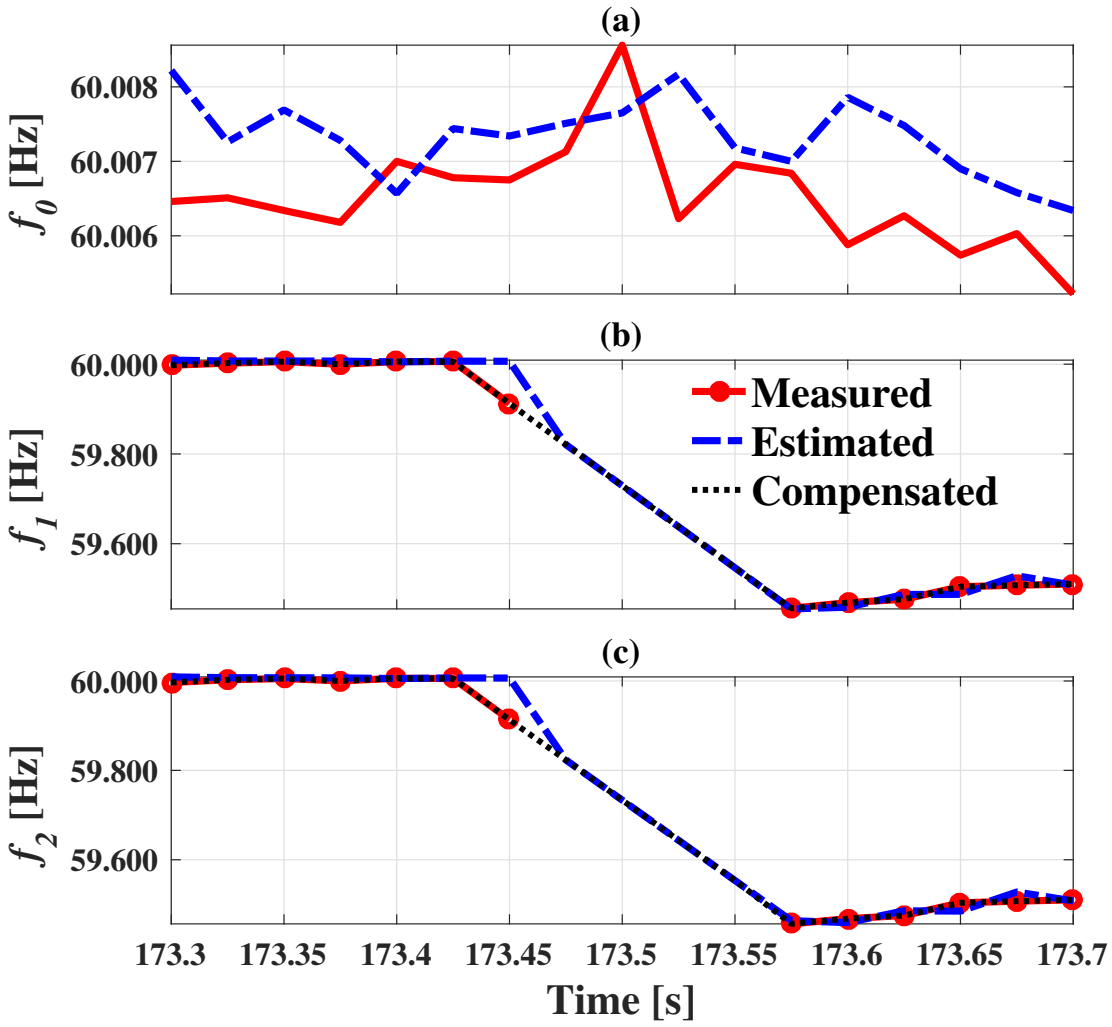

Figure 4.7 Performance of the proposed APDC regarding to islanding detection under successive packet dropouts for the two PMUs reporting DER measurements: (a) frequencies of the main PCC, (b) frequencies of DER 1, (c) frequencies of DER 2.

from DER_1 and DER_2 are dropped at exactly two data frames after islanding time, i.e., at $t = 173.475$ s. If there is no frequency estimation/compensation, then the first possible islanding detection would be at $t = 173.575$ s. i.e., 5 data frames later than that of detected if there were no packet dropouts. The detection delay is equal to 100 ms. However, employing the compensation unit, the missing data are substituted with the estimated values, as shown by the dashed line in Figures 4.7 (b) and (c). The detection unit alarms the islanding for both DERs at $t = 173.5$.

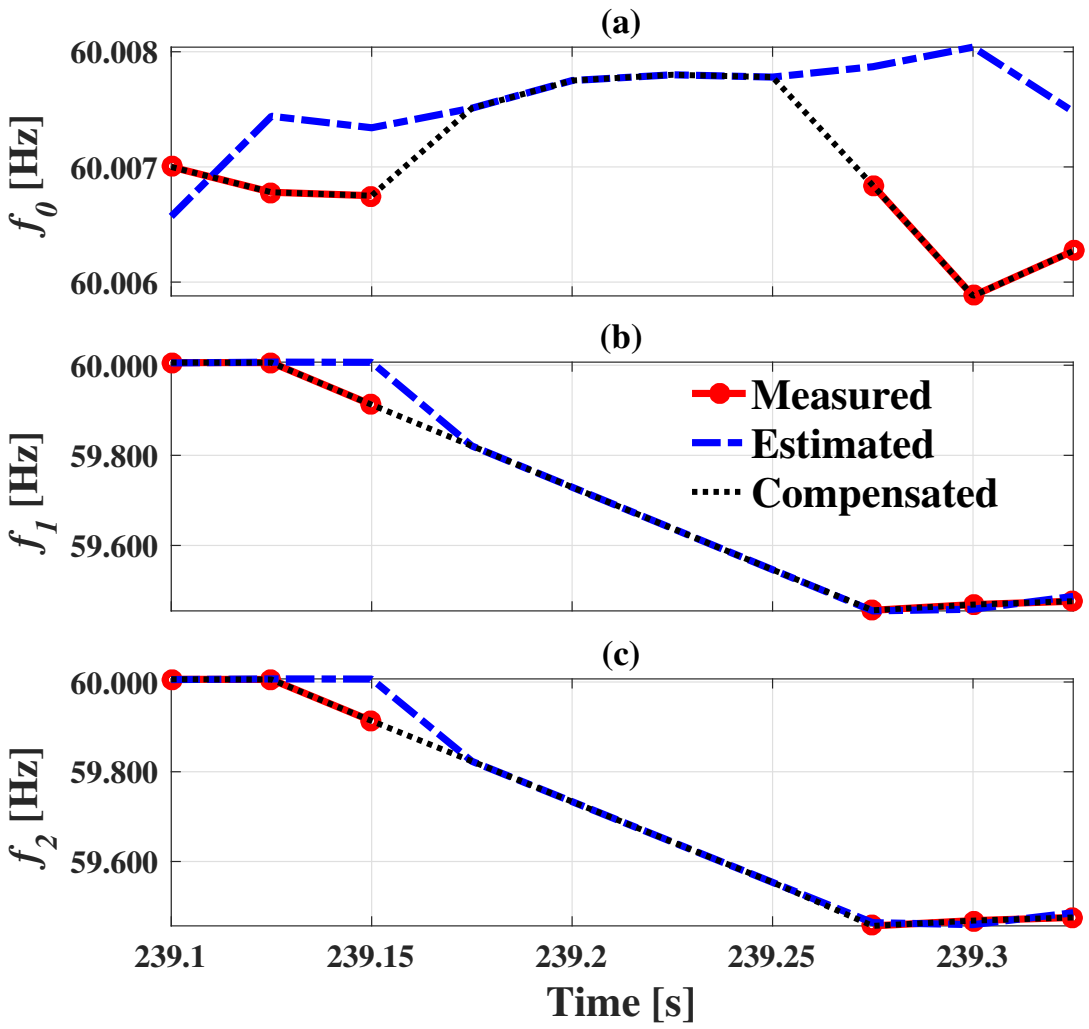

Figure 4.8 Performance of the proposed APDC regarding to islanding detection under successive packet dropouts for all the three PMUs: (a) frequencies of the main PCC, (b) frequencies of DER 1, (c) frequencies of DER 2.

Figure 4.8 (a)-(c) show the actual frequency data including the packet dropouts on the output of all three PMUs, the estimated frequencies, and the compensated data of f_0, f_1 and f_2. The two DER units are simultaneously islanded at $t = 239.125$ s. Four data packets from all PMUs are dropped at two data frames after islanding time, i.e., at $t = 239.175$ s. If there is no packet drop, then the islanding is detected at $t = 239.175$ s. However, with packet dropouts and no compensation unit, the first alarm will be at $t = 239.275$ s where the first data packet is received after 4 consecutive dropouts. By employing the compensation unit, the detection unit is abale to detect the contingency at $t = 239.2$ s with a delay of 25 ms.

4.4 Performance evaluation of APDC in the presence of noise

In Section 4.2, the performance of the LMMSE, the ROCOF-based and the adaptive estimators were evaluated using experimental results of the distribution network. It should be noted that the PMU input signals (i.e. voltages/currents of the distribution grid) were corrupted by unmeasurable noise. Therefore, the effect of noise on the FE of different estimation methods could not be explicitly studied. In this section, the frequency and the ROCOF measurements polluted with additive white Gaussian noise (AWGN) are used to determine the effect of noise and to evaluate the performance of estimators.

Table 4.3 shows the maximum FE values of PMU measurements and the maximum FE of outputs of estimation methods for different signal-to-noise ratios (SNRs) of PMU output frequency. The percentage of usage of ROCOF-based estimator (PRBE) is reported in Table 4.3 to evaluate the robustness of the adaptive estimator against the ROCOF noise.

It can be seen in Table 4.3, that the maximum FE of the LMMSE estimator is always lower than that of the PMU measurements. On the other hand, the maximum FE of the ROCOF-based estimator is higher than that of the PMU measurements. However, even for smaller SNRs, the ROCOF-based estimations do not differ significantly from those of the PMU measurements.

For frequencies with SNR value higher than 80 dB, the PRBE is almost equal to zero. Therefore, at most timestamps the adaptive estimator employs LMMSE, and consequently, the frequency estimations are highly accurate. However, for frequencies with SNR value lower than 80 dB, the PRBE increases. Hence, the maximum FE value of the adaptive estimator exceeds that of the PMU measurements due to the higher noise that affects the ROCOF measurements. Note that the effectiveness of the adaptive estimator lies on the trade-off

Table 4.3 Comparison of the maximum FE for different estimation methods in normal condition and in the presence of measurable noise [44].

SNR [dB]	PMU Max. Errors		Max. FE [mHz]			PRBE [%]
	RFE [Hz/s]	FE [mHz]	LMMSE	ROCOF-based	Adaptive	
80	1.3	22	13	46	46	0.4
75	2.6	44	27	91	91	14.4
70	4.2	69	43	144	144	36.5
60	11.8	196	120	406	406	74.4
50	46.4	789	473	1624	1624	93.1

between FE requirements under normal and disturbed conditions. The increased PRBE value during transients guarantees better estimations useful for monitoring and detection purposes. Moreover, the noise evaluation results show that the selected threshold $\Delta f_T = 0.15$ Hz is highly robust against noise, especially for SNR values greater than 70 dB.

It should be noted that by decreasing the SNR, the maximum RFE and the maximum FE values of PMU measurements increase drastically. By decreasing the SNR lower than 70 dB, the maximum FE of the PMU measurements even violates the requirements defined in [45]. For example, with SNR= 70 dB, the PMU output has a maximum FE of 0.069 Hz and a maximum RFE of 4.2 Hz/s that are not compliant with the synchrophasor standard. However, most commercial PMUs and especially the VIZIMAX PMU guarantee the compliant with requirements defined in the IEEE standard for synchrophasor measurements, even in the presence of noise. Therefore, PMU measured frequencies with SNRs lower than 70 dB are not likely to be seen in real-life.

4.5 Comparison with the interpolative method

Table 4.4 reports the comparison between the maximum FE of the adaptive estimator and that of the interpolative estimator proposed in [39] under steady-state conditions and ramp tests. In steady-state, with all the PMUs reporting nominal frequency $f_0 = f_1 = f_2 = 60$ Hz with SNR= 85 dB, both the adaptive and the interpolative estimators present lower maximum FE values comparing to that of the PMU measurements. However, the interpolative method has a slightly better performance in case of nominal frequencies. By increasing the noise (SNR= 70 dB), the interpolative estimator still has a better performance than the adaptive estimator.

Table 4.4 Comparison of the maximum FE of the adaptive and the interpolative estimation methods under steady-state and ramp tests [44].

Test conditions			Max. FE [mHz]		
	$f_{1,2}$ [Hz]	SNR [dB]	PMU	Interpolative	Adaptive
Steady-state $f_0 = 60$ Hz Test interval: 60 s	60	85	13.8	6.7	8.5
		70	69.3	33.8	144.0
	59.8	85	14.5	139.8	7.5
		70	72.6	165.7	146.3
Ramp range ±4 Hz $R_f = \pm 2$ Hz/s		85	48.8	3974.8	58.4
		70	85.7	3979.7	420.2

The key advantage of the adaptive estimator is in estimating off-nominal frequencies when for example the main grid frequency is at its nominal value ($f_0 = 60$ Hz) and the frequency of DERs have deviated to new values ($f_1 = f_2 = 59.8$ Hz). In such situations, the adaptive estimator has a superior performance over the interpolative estimator in both noisy (SNR= 85 dB) and very noisy (SNR= 70 dB) situations. This is because the interpolative method employs the average value of the frequencies of the three PMUs while the adaptive method utilizes the correlation between frequencies.

Furthermore, frequency ramp tests are conducted on f_1 and f_2 while fixing f_0 to 60 Hz. The PMU input terminals are supplied with sinusoids that have the general form of

$$x_i(t) = A_i(t)\cos\Big(2\pi f_n t + \pi R_f t^2 + \theta_i(t)\Big) \tag{4.1}$$

where the R_f is the frequency ramp rate in Hz/s that is the theoretical value of ROCOF for the given ramp slope [44].

The ramp rate is set to $R_f = \pm 2$ Hz/s and the frequency ramp is performed for 2 seconds resulting in a frequency change with the range of ± 4 Hz (from 58 to 60 Hz and contrariwise). As recommended by the IEEE standard [45], the first two reporting intervals (i.e. $2/F_s$) from both before the beginning and after the end of the ramp, are discarded and the rest are used for FE calculations. Table 4.4 compares the maximum FE of the two methods. It can be seen that the adaptive estimator successfully tracks the ramp frequency and even improves the maximum FE comparing to that of the PMU measurements when the SNR is 85 dB. However, the interpolative estimator has a very slow response with a poor maximum FE for both SNR values. The ramp test results further confirm the advantages of the proposed adaptive estimator under power system transients and disturbances.

To further investigate the advantages of the adaptive estimator in disturbed conditions, 4

Table 4.5 Detection delay time of APDC and interpolative method for packet dropouts performed on different PMUs.

Packet dropouts indicated by ✓			Detection time delay [ms]	
f_0	f_1	f_2	Interpolative	Adaptive
–	✓	–	25	0
–	✓	✓	100	25
✓	✓	–	75	0
✓	–	✓	75	0
✓	✓	✓	125	25

consecutive packet dropouts are performed on the outputs of different PMUs and the islanding detection results are evaluated. Table 4.5 shows the results of islanding detection regarding to the detection time delay. The detection time delay is calculated as the time delay between the timestamp at which alarm is set off and the actual timestamp at which the frequency measured by a PMU (without dropouts) violated the threshold value.

It can be seen in Table 4.5 that when packet dropouts occur only on the PMU of the DER 1, the adaptive estimator well compensates the dropouts and introduces no delay in detection the islanding event. However, the interpolative method detects the event with a 25 ms delay. Moreover, when both PMUs measuring the frequencies of DERs are subjected to packet dropouts, The interpolative method exhibits a 100 ms delay, while the detection delay of the APDC is 25 ms. Finally, when all the PMUs are subjected to packet dropouts, the detection time delay of the APDC is still 25 ms, whereas that of the interpolative method is increased to 125 ms.

CHAPTER 5 CONCLUSION

5.1 Summary

The primary objective of this thesis is the design and development of an APDC that enables monitoring of DERs in smart microgrids. The developed APDC is a software-based algorithm embedded in the conventional PDC allowing for an improvement of the data integrity, reliability, and the quality of the synchrophasor data reported by multiple PMUs installed within the smart grids. The APDC also utilizes the improved PMU datasets to monitor the smart grid and to detect abnormal events such as frequency excursion, islanding events, voltage instabilities, etc. The proposed APDC consists of two main units, namely the estimation/compensation unit and the monitoring/detection unit.

In Chapter 2, the concepts and the definition of synchrophasor data as well as PMU, a device capable of estimating and reporting synchrophasor data, are presented. The synchrophasor requirements of the PMU and different performance classes (i.e. P-class and M-class) defined in *IEEE Std. C37.118.1* are discussed, and various PMU performance criteria (i.e. TVE, FE, and RFE) are introduced in this chapter. The PDC that is responsible for collecting and sorting the synchrophasor data of multiple PMUs is introduced and its applications and multilayer structure are briefly described. The utilization of synchrophasor data and PDCs in WAMS and MCC are presented. Moreover, the synchrophasor messaging format and types defined in *IEEE Std. C37.118.1* are presented. Finally, OpenPDC as a software PDC including three adapter layers is presented and its capabilities and applications are discussed.

In Chapter 3, the proposed APDC is thoroughly detailed. The APDC includes two major sub-units that are estimation/compensation and monitoring/detection units. The estimation/compensation employs an adaptive estimator that can switch between a vector *linear minimum mean square error (LMMSE)* estimator and a derivative-based estimator sensitive to the rate of change of the parameter of interest. The basic idea of the adaptive estimator is to utilize the appropriate estimator under normal and disturbed operation conditions. Under the normal conditions (steady-state), the LMMSE estimator is utilized and for the disturbed conditions (transients), the derivative-based estimator is employed. At any time instant, the PMU measurements of the future time instant are predicted and are used if any communication loss or excessive delays occur. The compensated PMU data is then reported to the monitoring/detection unit for further processing. The monitoring/detection unit is developed to perform a centralized frequency excursion detection that processes the frequency data of DERs and the main grid to identify the islanded DERs. Note that , the proposed

monitoring/detection unit can be configured for many other applications such as voltage and power monitoring, DER protection and control, and microgrid energy management.

In Chapter 4, the experimental implementation of the proposed APDC is presented, and its performance is verified based on real-time synchrophasor data collected from three PMUs and different communication media. A test setup comprising three VIZIMAX PMUs and the proposed APDC developed using the OpenPDC software are implemented. The estimation/compensation unit is evaluated under normal and disturbed conditions with various levels of noise. The experiments confirm the advantages of the proposed adaptive estimator. The monitoring/detection is configured to detect frequency excursions and is tested under severe communication packet dropouts. The experimental results show that the proposed APDC has an excellent performance in terms of data integrity under both normal and disturbed conditions such as the presence of realistic measurement noise. The numerical results also confirm that the APDC can reliably monitor DERs and determine the islanded zones under consecutive packet dropouts. Finally, the performances of the proposed APDC and a recently proposed synchrophasor estimation method are compared under disturbed condition and communication losses. The comparison results further confirm the advantages of the proposed APDC.

5.2 Future work

The estimation/compensation unit of the APDC is the main contribution of this thesis. It succeeds to fulfill its purpose that is to improve the synchrophasor data integrity in several test cases of packet dropouts and delays in different conditions and different noise levels. It has been successfully verified with the real-time experimental data, real-time simulated data, and real-time emulated data. However, future work is required to verify the performance of the proposed unit in estimating voltage and currents as the target data elements. Moreover, additional tests are needed to prove the effectiveness of the proposed estimation/compensation unit in improving the synchrophasor data in case of PMU bad data estimations.

The monitoring/detection unit was only developed for islanding detection and frequency excursion detection cases. Further work is therefore required to investigate the effectiveness of the monitoring/detection unit in other applications such as voltage/current monitoring, DER unit protection and control, and microgrid energy management and control. It is also important to mention that this project was developed using three PMUs in VIZIMAX laboratories. The implementation of the proposed method using a greater number of PMUs installed in industrial environments will give a better verification of the proposed method.

Bibliography

[1] X. Fang, S. Misra, G. Xue, and D. Yang, "Smart grid - The new and improved power grid: A survey," *IEEE Commun. Surveys Tuts*, vol. 14, pp. 944–980, Fourth 2012.

[2] N. Hatziargyriou, H. Asano, R. Iravani, and C. Marnay, "Microgrids," *IEEE Power Energy Mag.*, vol. 5, pp. 78–94, July 2007.

[3] F. Katiraei, R. Iravani, N. Hatziargyriou, and A. Dimeas, "Microgrids management," *IEEE Power Energy Mag.*, vol. 6, pp. 54–65, May 2008.

[4] D. E. Olivares, A. Mehrizi-Sani, A. H. Etemadi, C. A. Canizares, R. Iravani, M. Kazerani, A. H. Hajimiragha, O. Gomis-Bellmunt, M. Saeedifard, R. Palma-Behnke, *et al.*, "Trends in microgrid control," *IEEE Trans. Smart Grid*, vol. 5, no. 4, pp. 1905–1919, 2014.

[5] A. H. K. Alaboudy, H. H. Zeineldin, and J. Kirtley, "Microgrid stability characterization subsequent to fault-triggered islanding incidents," *IEEE Trans. Power Del.*, vol. 27, pp. 658–669, April 2012.

[6] "IEEE guide for design, operation, and integration of distributed resource island systems with electric power systems," *IEEE Std 1547.4-2011*, pp. 1–54, July 2011.

[7] B. M. Eid, N. A. Rahim, J. Selvaraj, and A. H. E. Khateb, "Control methods and objectives for electronically coupled distributed energy resources in microgrids: A review," *IEEE Syst. J.*, vol. 10, pp. 446–458, June 2016.

[8] I. J. Balaguer, Q. Lei, S. Yang, U. Supatti, and F. Z. Peng, "Control for grid-connected and intentional islanding operations of distributed power generation," *IEEE Trans. Ind. Electron.*, vol. 58, pp. 147–157, Jan 2011.

[9] S.-I. Jang and K.-H. Kim, "An islanding detection method for distributed generations using voltage unbalance and total harmonic distortion of current," *IEEE Trans. Power Del.*, vol. 19, pp. 745–752, Apr. 2004.

[10] M. E. Ropp, M. Begovic, and A. Rohatgi, "Analysis and performance assessment of the active frequency drift method of islanding prevention," *IEEE Trans. Energy Convers.*, vol. 14, pp. 810–816, Sept. 1999.

[11] G.-K. Hung, C.-C. Chang, and C.-L. Chen, "Automatic phase-shift method for islanding detection of grid-connected photovoltaic inverters," *IEEE Trans. Energy Convers.*, vol. 18, pp. 169–173, Mar. 2003.

[12] W. Freitas, W. Xu, C. M. Affonso, and Z. Huang, "Comparative analysis between ROCOF and vector surge relays for distributed generation applications," *IEEE Trans. Power Del.*, vol. 20, pp. 1315–1324, Apr. 2005.

[13] H. Karimi, A. Yazdani, and R. Iravani, "Negative-sequence current injection for fast islanding detection of a distributed resource unit," *IEEE Trans. Power Electron.*, vol. 23, pp. 298–307, Jan. 2008.

[14] B. Bahrani, H. Karimi, and R. Iravani, "Nondetection Zone Assessment of an Active Islanding Detection Method and its Experimental Evaluation," *IEEE Transactions on Power Delivery*, vol. 26, pp. 517–525, Apr. 2011.

[15] M. E. Ropp, M. Begovic, A. Rohatgi, G. A. Kern, R. H. Bonn, and S. Gonzalez, "Determining the relative effectiveness of islanding detection methods using phase criteria and nondetection zones," *IEEE Trans. Energy Convers.*, vol. 15, pp. 290–296, Sept. 2000.

[16] M. Hamzeh, S. Emamian, H. Karimi, and J. Mahseredjian, "Robust control of an islanded microgrid under unbalanced and nonlinear load conditions," *IEEE Trans. Emerg. Sel. Topics Power Electron.*, vol. 4, pp. 512–520, June 2016.

[17] M. Babazadeh and H. Karimi, "A robust two-degree-of-freedom control strategy for an islanded microgrid," *IEEE Trans. Power Del.*, vol. 28, pp. 1339–1347, July 2013.

[18] J. Giri, "Proactive management of the future grid," *IEEE Power Energy Technol. Syst. J.*, vol. 2, pp. 43–52, June 2015.

[19] A. Ovalle, G. Ramos, S. Bacha, A. Hably, and A. Rumeau, "Decentralized control of voltage source converters in microgrids based on the application of instantaneous power theory," *IEEE Trans. Ind. Electron.*, vol. 62, pp. 1152–1162, Feb 2015.

[20] V. C. Gungor, D. Sahin, T. Kocak, S. Ergut, C. Buccella, C. Cecati, and G. P. Hancke, "Smart grid technologies: Communication technologies and standards," *IEEE Trans. Ind. Informat.*, vol. 7, pp. 529–539, Nov 2011.

[21] J. D. L. Ree, V. Centeno, J. S. Thorp, and A. G. Phadke, "Synchronized phasor measurement applications in power systems," *IEEE Trans. Smart Grid*, vol. 1, pp. 20–27, June 2010.

[22] A. Phadke and J. Thorp, *Synchronized Phasor Measurements and Their Applications*. Power Electronics and Power Systems, Springer US, 2010.

[23] A. Monti, F. Ponci, and C. Muscas, *Phasor Measurement Units and Wide Area Monitoring Systems*. Elsevier Science & Technology Books, 2016.

[24] R. F. Nuqui and A. G. Phadke, "Phasor measurement unit placement techniques for complete and incomplete observability," *IEEE Trans. Power Del.*, vol. 20, pp. 2381–2388, Oct 2005.

[25] B. Milosevic and M. Begovic, "Nondominated sorting genetic algorithm for optimal phasor measurement placement," *IEEE Trans. Power Syst.*, vol. 18, pp. 69–75, Feb 2003.

[26] B. Gou, "Generalized integer linear programming formulation for optimal pmu placement," *IEEE Trans. Power Syst.*, vol. 23, pp. 1099–1104, Aug 2008.

[27] A. von Meier, D. Culler, A. McEachern, and R. Arghandeh, "Micro-synchrophasors for distribution systems," in *ISGT 2014*, pp. 1–5, Feb 2014.

[28] X. Chen, K. J. Tseng, and G. Amaratunga, "State estimation for distribution systems using micro-synchrophasors," in *2015 IEEE PES Asia-Pacific Power and Energy Engineering Conference (APPEEC)*, pp. 1–5, Nov 2015.

[29] B. Pinte, M. Quinlan, and K. Reinhard, "Low voltage micro-phasor measurement unit (μPMU)," in *2015 IEEE Power and Energy Conference at Illinois (PECI)*, pp. 1–4, Feb 2015.

[30] Y. Deng, H. Lin, A. G. Phadke, S. Shukla, J. S. Thorp, and L. Mili, "Communication network modeling and simulation for wide area measurement applications," in *2012 IEEE PES Innovative Smart Grid Technologies (ISGT)*, pp. 1–6, Jan 2012.

[31] G. Sanchez-Ayala, J. R. Aguerc, D. Elizondo, and M. Lelic, "Current trends on applications of pmus in distribution systems," in *2013 IEEE PES Innovative Smart Grid Technologies Conference (ISGT)*, pp. 1–6, Feb 2013.

[32] D. Shi, Y. Luo, and R. K. Sharma, "Active synchronization control for microgrid reconnection after islanding," in *IEEE PES Innovative Smart Grid Technologies, Europe*, pp. 1–6, Oct 2014.

[33] A. Borghetti, C. A. Nucci, M. Paolone, G. Ciappi, and A. Solari, "Synchronized phasors monitoring during the islanding maneuver of an active distribution network," *IEEE Trans. Smart Grid*, vol. 2, pp. 82–91, Mar. 2011.

[34] Y. Guo, K. Li, D. M. Laverty, and Y. Xue, "Synchrophasor-based islanding detection for distributed generation systems using systematic principal component analysis approaches," *IEEE Trans. Power Del.*, vol. 30, pp. 2544–2552, Dec 2015.

[35] Z. Ye, A. Kolwalkar, Y. Zhang, P. Du, and R. Walling, "Evaluation of anti-islanding schemes based on nondetection zone concept," *IEEE Trans. Power Electron.*, vol. 19, pp. 1171–1176, Sept. 2004.

[36] L. A. C. Lopes and H. Sun, "Performance assessment of active frequency drifting islanding detection methods," *IEEE Trans. Energy Convers.*, vol. 21, pp. 171–180, Mar. 2006.

[37] Z. Lin, T. Xia, Y. Ye, Y. Zhang, L. Chen, Y. Liu, K. Tomsovic, T. Bilke, and F. Wen, "Application of wide area measurement systems to islanding detection of bulk power systems," *IEEE Trans. Power Syst.*, vol. 28, pp. 2006–2015, May 2013.

[38] H. Karimi, H. Nikkhajoei, and R. Iravani, "Control of an electronically-coupled distributed resource unit subsequent to an islanding event," *IEEE Trans. Power Del.*, vol. 23, pp. 493–501, Jan. 2008.

[39] Y. Seyedi, H. Karimi, and J. Guerrero, "Centralized disturbance detection in smart microgrids with noisy and intermittent synchrophasor data," *IEEE Trans. Smart Grid*, vol. PP, no. 99, pp. 1–1, 2016.

[40] Y. Seyedi, H. Karimi, and S. Grijalva, "Distributed generation monitoring for hierarchical control applications in smart microgrids," *IEEE Trans. Power Syst.*, vol. PP, no. 99, pp. 1–1, 2016.

[41] E. Cotilla-Sanchez, P. D. H. Hines, and C. M. Danforth, "Predicting critical transitions from time series synchrophasor data," *IEEE Trans. Smart Grid*, vol. 3, pp. 1832–1840, Dec 2012.

[42] S. Das and T. S. Sidhu, "Application of compressive sampling in synchrophasor data communication in wams," *IEEE Trans. Ind. Informat.*, vol. 10, pp. 450–460, Feb 2014.

[43] M. Wu and L. Xie, "Online detection of low-quality synchrophasor measurements: A data driven approach," *IEEE Trans. Power Syst.*, vol. PP, no. 99, pp. 1–1, 2016.

[44] R. Pourramezan, Y. Seyedi, H. Karimi, G. Zhu, and M. Mont-Briant, "Design of an advanced phasor data concentrator for monitoring of distributed energy resources in smart microgrids," *IEEE Trans. Ind. Informat.*, 2017. doi: 10.1109/TII.2017.2697438.

[45] "IEEE standard for synchrophasor measurements for power systems," *IEEE Std C37.118.1-2011 (Revision of IEEE Std C37.118-2005)*, pp. 1–61, Dec 2011.

[46] P. Kundur, N. J. Balu, and M. G. Lauby, *Power system stability and control*. New York: McGraw-Hill, 1994. OCLC: 28929603.

[47] D. R. Gurusinghe, A. D. Rajapakse, and K. Narendra, "Testing and Enhancement of the Dynamic Performance of a Phasor Measurement Unit," *IEEE Trans. Power Del.*, vol. 29, pp. 1551–1560, Aug. 2014.

[48] C. I. Chen, "A phasor estimator for synchronization between power grid and distributed generation system," *IEEE Trans. Ind. Electron.*, vol. 60, pp. 3248–3255, Aug 2013.

[49] N. Jaleeli and L. VanSlyck, "Control performance standards and procedures for interconnected operation," *EPRI TR-107813*, Apr. 1997.

[50] L. R. Chang-Chien, Y. S. Wu, and J. S. Cheng, "Online estimation of system parameters for artificial intelligence applications to load frequency control," *Transmission Distribution IET Generation*, vol. 5, pp. 895–902, Aug. 2011.

[51] "IEEE standard for synchrophasor data transfer for power systems," *IEEE Std C37.118.2-2011 (Revision of IEEE Std C37.118-2005)*, pp. 1–53, Dec 2011.

[52] *GridProtectionAlliance/The Open Phasor Data Concentrator*. [Online]. Available: https://github.com/GridProtectionAlliance/openPDC/.

[53] L. I. Minchala-Avila, L. Garza-Castañón, Y. Zhang, and H. J. A. Ferrer, "Optimal energy management for stable operation of an islanded microgrid," *IEEE Trans. Ind. Informat.*, vol. 12, pp. 1361–1370, Aug. 2016.

[54] S. M. Kay, *Fundamentals of Statistical Processing, Volume I: Estimation Theory*. Englewood Cliffs, N.J: Prentice Hall, Mar. 1993.

[55] T. Kato, T. Inoue, and Y. Suzuoki, "Estimation of total power output fluctuation of high penetration photovoltaic power generation system," in *2011 IEEE Power and Energy Society General Meeting*, pp. 1–7, July 2011.

[56] N. Jaleeli and L. S. VanSlyck, "NERC's new control performance standards," *IEEE Trans. Power Syst.*, vol. 14, pp. 1092–1099, Aug. 1999.

[57] Y. G. Rebours, D. S. Kirschen, M. Trotignon, and S. Rossignol, "A survey of frequency and voltage control ancillary services mdash;part i: Technical features," *IEEE Trans. Power Syst.*, vol. 22, pp. 350–357, Feb 2007.

[58] *Measure, control and switch – solutions for HV-MV power systems.* [Online]. Available: http://vizimax.com/.

[59] J. Mahseredjian, S. Dennetière, L. Dubé, B. Khodabakhchian, and L. Gérin-Lajoie, "On a new approach for the simulation of transients in power systems," *Electric Power Systems Research*, vol. 77, pp. 1514–1520, Sept. 2007.